This is to certify that the

dissertation entitled

X-RAY CRYSTALLOGRAPHIC STUDIES OF MIP SYNTHASE

presented by

Adam J. Stein

has been accepted towards fulfillment
of the requirements for

PhD degree in Chemistry

Major professor

Date 4/3/02

DATE DUE	DATE DUE	DATE DUE

X-RAY CRYSTALLOGRAPHIC STUDIES OF MIP SYNTHASE

By

Adam Joshua Stein

A DISSERTATION

Submitted to

Michigan State University
In partial fulfillment of the requirements
for the degree of

DOCTOR OF PHILOSOPHY

Department of Chemistry

2002

ABSTRACT

X-RAY CRYSTALLOGRAPHIC STUDIES OF MIP SYNTHASE

By

Adam Joshua Stein

1L-*myo*-inositol 1-phosphate synthase catalyzes the conversion of D-glucose 6-phosphate to 1L-*myo*-inositol 1-phosphate. This represents the first step in the biosynthesis of all inositol-containing compounds. The reaction involves a complex series of transformations including oxidation, intramolecular aldol condensation, and reduction, all of which occur in the same active site of the enzyme. Two crucial crystal structures of MIP synthase have been solved: (1) the holo form and (2) an enzyme/inhibitor complex with the inhibitor, 2-deoxy-glucitol 6-phosphate. While 58 amino acids are disordered in the holo form of the enzyme near the active site, the inhibitor nucleates the folding of this domain serving to completely encapsulate it within the enzyme. Three helices and a long beta strand are formed in this process. A mechanism for this binding is proposed that first involves the binding of the inhibitor to the ordered part of the enzyme followed by the nucleation and folding of the disordered region. We further postulate a mechanism for the conversion based on the structure of the inhibitor-bound complex.

To my wife, for all of your love and support in finishing this part of my life.

ACKNOWLEDGEMENTS

I would like to acknowledge all the people that have helped me get to this point. First and foremost, I would like to thank my advisor, Dr. James H. Geiger. Without your intellect and guidance, this thesis would not be possible. Thanks for all the times spent on the graphics trying to figure out the final resting place of the inhibitor. In addition, thanks for helping me become a better scientist and more importantly, a good crystallographer.

I would also like to acknowledge the support of my coworkers, past and present members of the Geiger group, for their friendship, helpful discussions, and encouragement. More specifically, I would like to sincerely thank Marta C. Abad and Stacy Hovde for all the lunches, advice, and discussions involving our structures. To both of you, good luck with all your endeavors in whatever road you choose to travel.

I am deeply indebted to Dr. Alexander Tulinsky and Dr. Jorge Rios for steering me in the right direction. Doc, your knowledge and insight have inspired me. Jorge, you showed me the essentials and for that, I will always remember you.

I would also like to say thanks to Dr. John W. Frost and Chad Hansen for supplying the inhibitors for this study and for the verification of MIP synthase sequence. Without you guys, we would probably still be wondering where the remaining fifty-residues were.

Financially, I would like to thank both the NSF and the MSU IRGP for funding this project. Without their support, this project would not have been possible.

Finally, I would like to thank my family and most importantly, my wife. Without you Shannon, life would be empty. Your help and support over the years have enabled me to make this possible and I want you to know that. Whenever I had an issue or a problem, you were there for me to lean on. Just remember that I will love you "always and forever."

TABLE OF CONTENTS

LIST OF TABLES

LIST OF FIGURES

** Some of the images in this dissertation are presented in color.

LIST OF ABBREVIATIONS

MIP	*myo*-inositol 1-phosphate
NAD	nicotinamide adenine dinucleotide
NADH	nicotinamide adenine dinucleotide, reduced form
MI/Ins	*myo*-inositol
CDP-DAG	cytodine diphosphate-diacylglycerol
PtdIns	phosphatidyl inositol
PtdIns(4,5)P_2	phosphatidylinositol-4,5-bisphosphate
Ins(1,4,5,)P_3	*myo*-inositol-1,4,5-triphosphate
GDP	guanosine diphosphate
GTP	guanosine triphosphate
PLC-β	phospholipase C-β
ER	endoplasmic reticulum
GPI	glycosyl phosphatidyl inositol
DAPDH	diaminopimilate dehydrogenase
G6P	D-glucose 6-phosphate
DHQ	dehydroquinate synthase
NADPH	nicotinamide adenine dinucleotide phosphate, reduced form
SQD1	sulfolipid biosynthesis protein
NaAc	sodium acetate
PEG	polyethylene glycol
Se	selenium

Se-Met	seleno-methionine
MAD	multi-wavelength anomalous dispersion
LB	Lauria-Bertani medium
AMP	ampicillin
IPTG	isopropy-β-D-thiogalactopyranoside, dioxane free
BME	β-mercaptoethanol
TCA	trichloroacetic acid
$NaIO_4$	sodium periodate
Na_2SO_3	sodium sulfite
DTT	dithiothreitol
ddH_2O	double distilled water
dgtolP	2-deoxy-glucitol 6-phosphate
MIR	multiple isomorphous replacement
p-CMB	para-chloromercuriobenzoate
FOM	figure of merit
ALDH	aldehyde dehydrogenase
OXRED	oxidoreductase
UPS	undecaprenyl pyrophosphate synthase
ADH	alcohol dehydrogenase
PKC	protein kinase C

CHAPTER 1

INTRODUCTION

BACKGROUND

General Overview

myo-Inositol is the starting material for the biosynthesis of a host of critically important signaling molecules including the poly-phosphorylated *myo*-inositols and the precursor phosphoinositides[1]. *myo*-Inositol 1-phosphate synthase (MIP synthase, EC 5.5.1.4) converts D-glucose 6-phosphate to *myo*-inositol 1-phosphate. This is the first committed and rate limiting step in the *de novo* biosynthesis of all inositols in eukaryotes[2]. This complex transformation occurs via a multi-step reaction mechanism involving an oxidation, reduction, and intramolecular aldol condensation. This mechanism occurs stereospecifically within a single active site with no dissociation of intermediates. The aldol condensation is novel in that it seems to involve neither lysine Schiff-base formation nor metal activation, rather a monovalent cation for catalysis[3]. A more detailed mechanism analysis will be presented in a later section.

MIP synthase is found in many eukaryotes including protozoa, fungi, algae, plants, mammals, and humans. The gene encoding MIP synthase has been cloned from several organisms including yeast (*INO1* gene), amoebas, and several plants[4,37]. In all organisms, MIP synthase codes for an approximate 60 kD monomer polypeptide. Very homologous complete sequence data has been obtained, via a BLAST search, from mice and humans as well[5].

MIP synthase is a member of a unique class of enzymes that use NAD not as a cosubstrate, but as a co-catalyst[6]. NAD is reduced to NADH and then reoxidized back to NAD in the same catalytic cycle. Though a mechanistic scheme has been proposed, there was no structural data illuminating the details of this enzyme's precise role in this important conversion until the inhibitor/MIP structure was solved. Even though the three-dimensional fold of the protein is now known, the enzyme's amino acid sequence has no homology to proteins which utilize a NAD-binding domain.

Strikingly, MIP synthase may be a target of therapeutic importance. Currently, lithium is used in the treatment of manic depression[7]. Although the precise mechanism by which this occurs is unknown, one theory is that lithium acts by inhibiting MIP phosphatase and reducing inositol levels in the brain. Other inhibitors of the phosphatase have already been tested in animal models and are found to have similar effects to those of lithium, adding credence to this mode of action[8]. Inhibiting MIP synthase may also lower inositol levels in the brain and have a similar therapeutic effect. Recent data seems to suggest that valproate may inhibit the MIP synthase pathway[53].

Inositols and Cellular Signaling

myo-Inositol (MI or Ins.) is a critical component of all eukaryotic membranes. The *de novo* biosynthesis of *myo*-inositol begins with the conversion of glucose 6-phosphate to *myo*-inositol 1-phosphate (MIP) by MIP synthase, followed by dephosphorylation of this product by MIP phosphatase to give *myo*-

inositol (Figure 1). MI is then combined with cytodine diphosphate-diacylglycerol (CDP-DAG) in a reaction catalyzed by phosphatidyl inositol synthase to form phosphatidyl inositol (PtdIns)[9]. PtdIns is the most abundant inositol lipid in nature, making up 5% of the total membrane phospholipid content in eukaryotes[1]. Subsequent phosphorylations on the inositol moiety of PtdIns produce a variety of polyphosphorylated inositides including phosphatidylinositol-4,5-bisphosphate (PtdIns(4,5)P_2), which is the precursor of a central second messenger, *myo*-inositol 1,4,5-triphosphate (Ins(1,4,5)P_3) (Figure 1).

This second messenger is released when extracellular agonists bind to a heterotrimeric G-protein-coupled receptor, causing the exchange of GDP for GTP and subsequent activation of phospholipase C-β (PLC-β). Hydrolysis of PtdIns(4,5)P_2 by activated PLC-β liberates Ins(1,4,5)P_3, which binds to its receptor buried in the membrane of the endoplasmic reticulum (ER) and stimulates the release of Ca^{+2}. Ca^{+2} release in turn causes a diverse set of cellular responses including secretion, excitation, contraction, growth, and proliferation[10]. MIP synthase's role in this process is to maintain the concentration of *myo*-inositol necessary for these critical signal transduction processes to occur. The pathway described above is depicted in Figure 1.

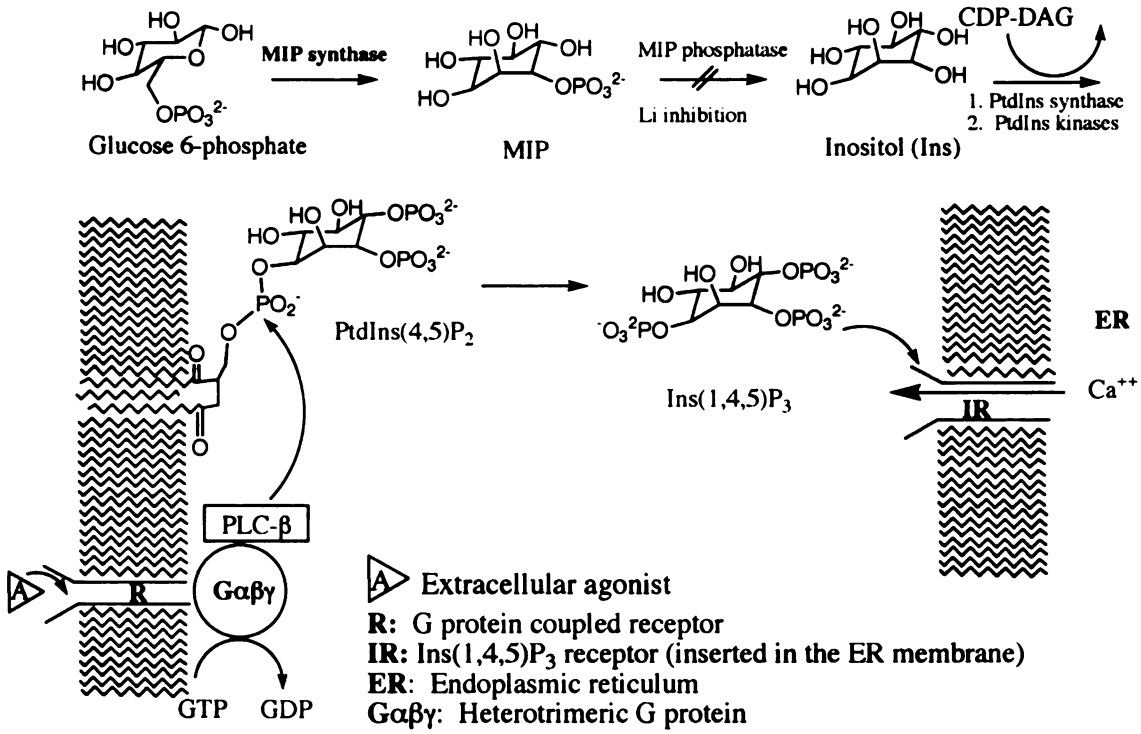

Figure 1. The biosynthesis of inositols and inositol phosphates.

The Biological Role of MIP Synthase Activity

Recent studies have focused on the regulation of the enzyme *in vivo* in both plants and fungi. In the latter case, the transcriptional regulation of the gene has proven to be both complex and responsive. Transcription of the yeast *INO1* gene is repressed in the presence of an inositol source and responds in an intricate manner to the levels of the various inositol-phospholipids and their precursors, inositol and choline[11-15]. Several transcription factors have been implicated in the process, including both those that appear to be specific for phosphoinositide biosynthesis, as well as those that are involved in regulation of other genes as well[16-22]. These studies show that the activity of MIP synthase is carefully regulated in response to cellular environment and stress. These studies also show this activity to be an important determinant in cellular regulation in yeast.

Recent studies in plants have demonstrated that MIP synthase plays several critical roles in these organisms as well. MIP synthase activity has been shown to be rapidly up regulated by the plant growth hormone abscisic acid during hormone–induced morphogenic response[4f]. MIP synthase also plays an essential role in seed development in rice by directing the synthesis of phytin both chronologically and temporally[23]. MIP synthase is also differentially regulated during embryonic and post-embryonic development of *P. vulgaris*[24].

Inositol metabolism plays an important role in plant salinity tolerance. The inositol metabolites ononitol and pinitol, as well as inositol itself, lower the cytoplasmic osmotic potential and balance sodium accumulation in the vacuole.

MIP synthase's role in this response is not merely in synthesizing the precursor MIP, but also in regulating sodium uptake in the roots with photosynthetic activity in the leaves. The enzyme is expressed in high levels in the leaves, maintains a gradient in the phloem, and is down regulated in the roots. This causes root growth and concomitant salt uptake to be dependent on the plant's capacity to produce glucose by photosynthesis. The glucose is then converted to *myo*-inositol by MIP synthase and freely transported to the roots via the phloem. In short, MIP synthase activity is thought to be the linchpin of an important regulatory system in plants, intimately involved in communication between photosynthetic activity and root metabolism[4c, 25-26].

All of this data indicates that MIP synthase activity plays important roles in plant development, response to environmental stress, long-range communication, and intracellular signaling. Interest in the role of these enzymes in plant biology is intensifying as most of these results have come within the last decade[27].

More recently, MIP synthase has been cloned from a parasitic protozoan *Entamoeba histolytica*. The enzyme's action is critical to the parasitic function of these organisms because they use glycosyl phosphatidyl inositol (GPI) to anchor macromolecules to their exterior membrane. Also, by changing the *E. histolytica* MIP synthase gene, the evolution of MIP synthase along the phylogenetic line may be traced. Many of these macromolecules are necessary for interaction with the target host[28].

Even though the gene encoding for MIP synthase in mice and humans has been cloned, little is known regarding the regulation of this enzyme in these higher eukaryotes. Indeed, since most of the inositols in mammals and higher eukaryotes come from dietary sources, it is not expected that the enzyme will be generally expressed. However, MIP synthase activity exists and can be purified from rat and bovine testis, rat and human brain, rat liver and kidneys, and rat mammary gland[29-31]. MIP synthase activity in the liver is reduced by thyroid removal, but this reduction can be reversed by hormone treatment[32]. This indicates that MIP synthase may be part of an important regulatory pathway in some organs. Since dietary inositol does not traverse the blood/brain barrier, MIP synthase activity is probably important in maintaining inositol levels there, especially since brain and nerve tissue actively use Ins(1,4,5)P_2 as a second messenger in neuronal stimulation. Several reports have shown that changes in brain inositol levels can have profound effects on various aspects of behavior, indicating that inositol synthesis is an important determinant of neurochemical brain function[8a, 33-36].

In short, all of the available data indicates that MIP synthase behaves not as a housekeeping gene, whose expression and activity remain level through the life of the cell, but as a gene that has important *regulatory* functions in response to stress, cellular signaling, and development.

MIP Synthase Homology, Classification, and Characteristics

The amino acid sequence of MIP synthase has been remarkably well conserved throughout evolution, from archae to human, over virtually its entire sequence[2]. For example, the *S. cerevisae* (yeast) and *D. melanogaster* (fly) amino acid sequences are 45% identical in overall sequence. Similarly, with the archae species, there is also a high sequence homology. Interestingly, in the active site, the yeast and archae species are 75% homologous even though the overall sequences differ by 150 amino acids. In contrast to this high homology, BLAST searches of all available gene databases using the Stanford yeast MIP synthase sequence reveal convincing homology to all other MIP synthase genes whose sequences are known, but show no convincing homology to any other protein[5]. In addition, the amino acid sequence of MIP synthase was subjected to a battery of threading and fold-recognition programs available from the UCLA-DOE structure prediction server[38], and again, no convincing matches were found. There was one interesting result from the folding recognition searches. The enzyme diaminopimilate dehydrogenase (DAPDH), an enzyme involved in L-arginine synthesis, has no sequence homology but does have similar folds. This enzyme consists of a Rossmann-fold, dimerization interface, and an insertion domain, each characteristic of the MIP synthase structure. These results are in agreement with those of the literature, suggesting that MIP synthase is structurally unique[2]. Figure 2 depicts the sequence alignment between all known species of MIP synthase.

MIP synthase is a member of a small class of enzymes that utilize NAD catalytically. This class of enzymes includes the epimerases, nucleoside diphosphohexose oxidoreductase, *S*-adenosylehomocysteine hydrolase, dehydroquinate synthase (DHQ synthase), SQD1, and ornithine cyclase[39]. The strategy of all these enzymes is to transiently oxidize an alcohol or amine to a carbonyl or imine. Carbon-carbon bonds are either formed or broken at positions adjoining the oxidized group. NADH or NADPH then reduces the oxidized group back to its original form to complete the catalytic cycle. Of all of these enzymes, the X-ray structures of DHQ synthase, UDP-galactose-4-epimerase, SQD1, and *S*-adenosylehomocysteine hydrolase are known[40-43]. While the epimerase and SQD1 have similar overall folds, both DHQ synthase and *S* – adenosylehomocysteine hydrolase are structurally unique. The one structural characteristic that all of these enzymes share is a Rossmann fold-like NAD binding domain. Even though these enzymes share an NAD-binding domain in their structures, no convincing sequence homology can be detected between it and any of these enzymes in pairwise alignments using the DNASTAR program package.

In most cases, the MIP synthase gene encodes for a protein of around 530 amino acids (533 in yeast) corresponding to a subunit weight of around 60 kD. Purification and characterization of both native and recombinant proteins from several species have demonstrated several salient features of the enzyme:

(a) It is always oligomeric in solution. While the chloroplast and fungal enzymes are trimers, most other forms behave as tetramers.

(b) It is activated by ammonium ions (five fold) and inhibited by glucitol 6-phosphate, 2-deoxy-glucose 6-phosphate, and *E*-vinylhomophosphonate.
(c) It operates in a pH range of 7.0-8.4.
(d) Requires NAD for activity, but uses it catalytically, not as a co-substrate.

As the crystal structures of MIP synthase will show, features (a) and (b) are essential in understanding the chemistry behind MIP synthase catalysis. These features demonstrate how similarly the enzyme behaves from species to species. The combination of the high sequence conservation shown above, and the fact that the enzymes behave so similarly, imply that structural insights will be immediately transferable to other MIP synthase enzymes from other organisms based on the structure of the yeast MIP synthase.

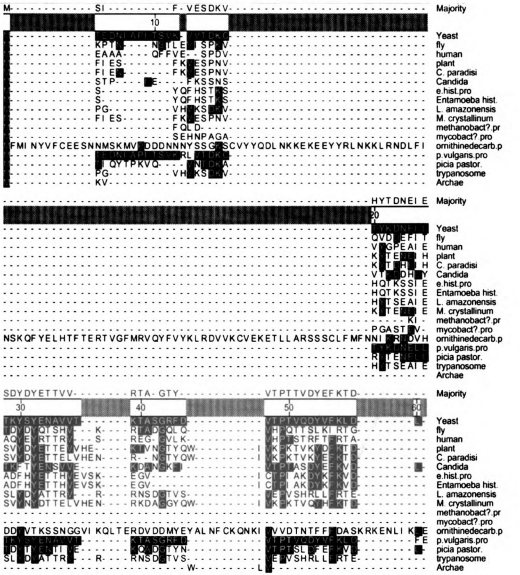

Figure 2. Sequence homology between several MIP synthase species.

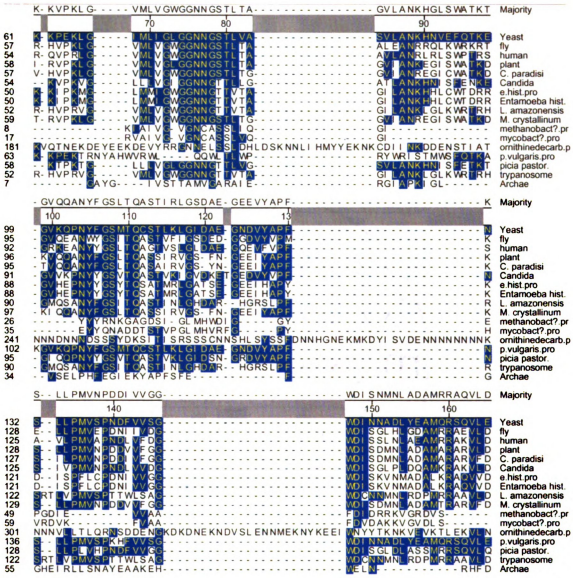

Figure 2 (cont'd)

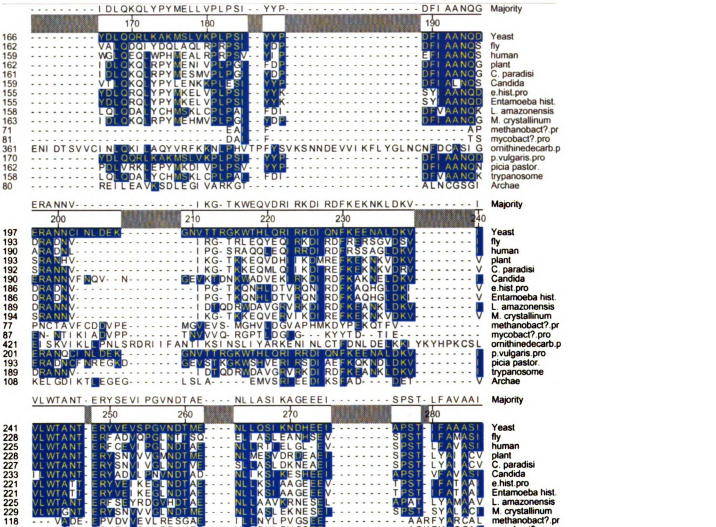

Figure 2 (cont'd)

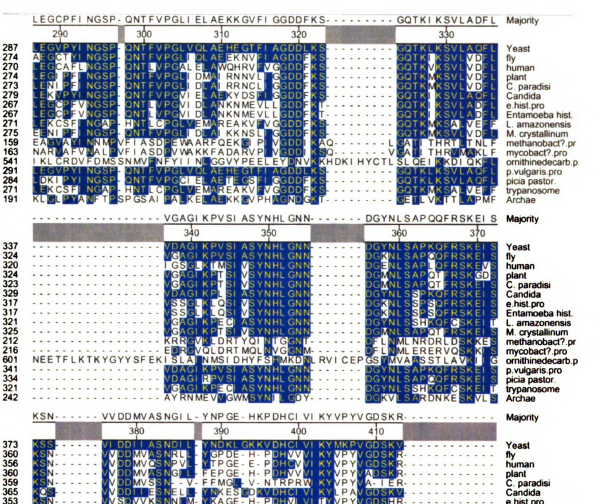

Figure 2 (cont'd)

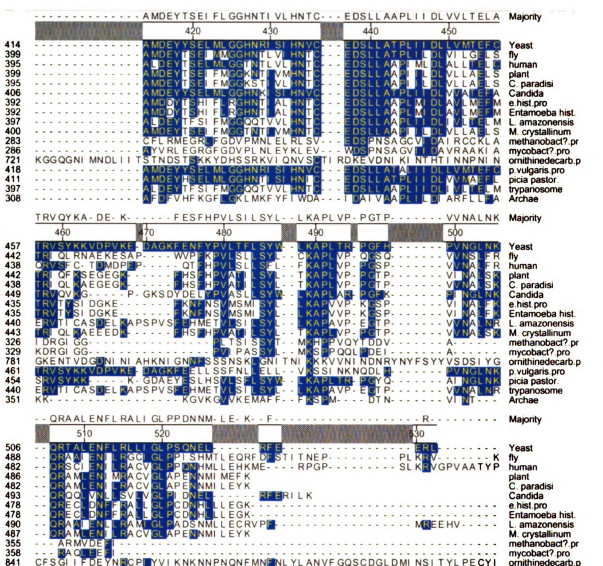

Figure 2 (cont'd)

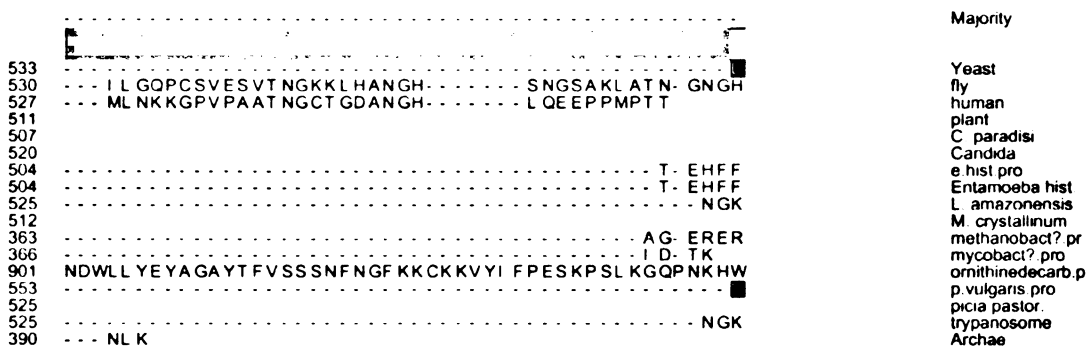

Figure 2 (cont'd)

Mechanistic Aspects of MIP Synthase

The elucidation of the intricate set of reactions catalyzed in the active site of MIP synthase has been the subject of intense investigation for the past thirty years. These studies have involved the use of radiolabeled substrate and NAD in feeding and biochemical studies, as well as mechanism based inhibitors[2, 39, 44-45]. Mechanistic studies indicate that MIP synthase from various sources share the common mechanism originally predicted by Loewus and Kelly[6b]. These experiments have resulted in the proposed mechanism shown in Figure 3.

The first step of this process is either binding of the acyclic form of glucose 6-phosphate or binding of the more prevalent cyclic form followed by acid or base catalyzed ring opening in the active site. NAD then oxidizes this acyclic compound in the C-4 position to yield the keto intermediate B. Enolization of this ketone to form intermediate C sets up the cyclization reaction by aldol condensation to yield D. NADH then reduces the C-5 keto group back to an alcohol and enzyme release yields the product 1L-*myo*-inositol 1-phosphate.

The mechanistic studies were carried out with partially purified enzymes obtained from different sources. Most of the findings were similar with regard to the mechanism, suggesting a similar mechanism for all species. Initial mechanistic studies concluded that *myo*-inositol 1-phosphate synthase requires NAD for activity. Treatment with charcoal removes NAD from the rat testis enzyme, leaving a totally inactive apoenzyme[74, 101, 102]. Reconstitution of the apoenzyme with added NAD restores 80% of the original activity. NADH generated during the reaction is tightly bound to the enzyme and therefore does

not seem to be exchanged between the enzyme-bound NADH and free NADH in the medium. The hydrogen on the C-5 of D-glucose 6-phosphate (G6P) is transferred to the C-4 position of the dihydropyridine ring of NADH during the oxidation of G6P, and the same hydrogen is delivered back to the product at the same position during the reduction of 2-inosose 1-phosphate. Adding NADH(^{3}H) to an incubation medium of MIP synthase and G6P failed to introduce tritium into the reaction substrate and product[101, 103]. None of the intermediates have been isolated, suggesting all intermediates are tightly bound and not released until the final reduction to *myo*-inositol 1-phosphate. When *myo*-inositol 1-phosphate synthase from bovine testis was incubated simultaneously with a mixture of deuterated D-glucose 6-phosphate-d_7 and nondeuterated D-glucose 6-phosphate-d_0, there was no crossover of the label from deuterated to nondeuterated product[104].

Incubation of partially purified apoenzyme from rat testis with 5-keto-G6P and [RS-4-^{3}H]-NADH led to the formation of D-glucose 5-^{3}H 6-phosphate and trace levels of tritiated *myo*-inositol 1-phosphate[102]. This apoenzyme also catalyzed the reduction of 5-keto-D-glucitol 6-phosphate by [RS-4-^{3}H]-NADH to form D-glucitol 5-^{3}H 6-phosphate. Additional evidence for the involvement of 5-keto-G6P was found in another experiment in which base treatment of 5-keto-G6P yielded two cyclose phosphates, which after reduction with $NaBH_4$, gave a mixture of two cyclitol monophosphates, L-*myo*-inositol 1-phosphate and *epi*-inositol 3-phosphate[105].

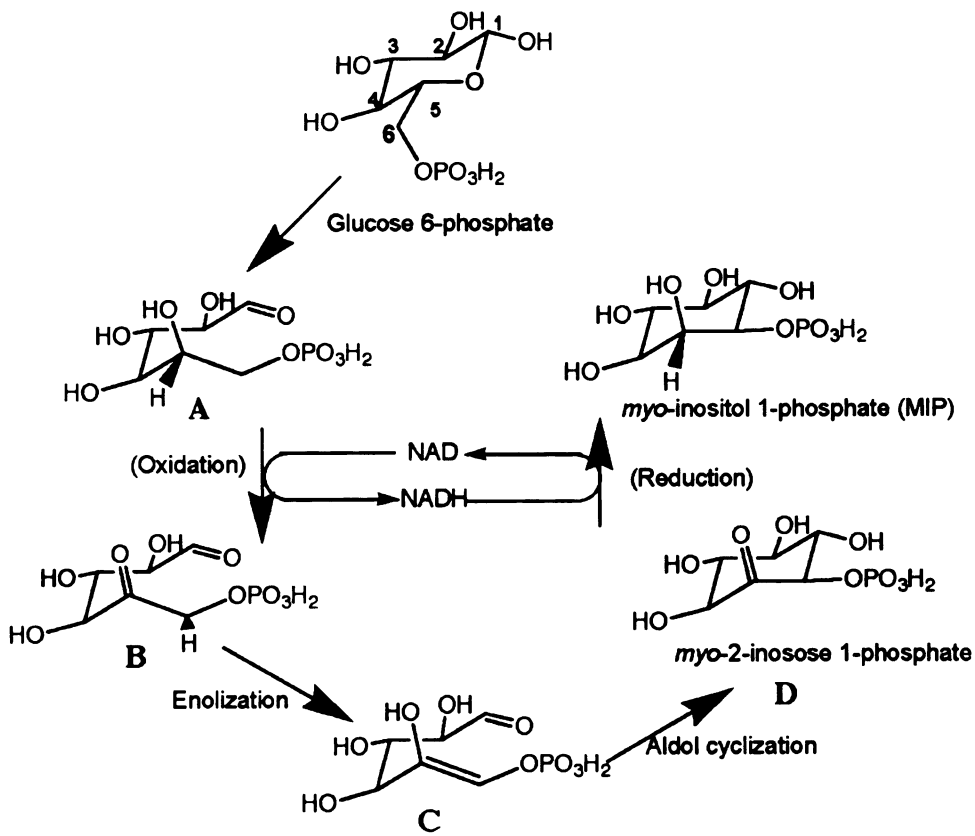

Figure 3. The proposed mechanism of MIP synthase.

By addition of NaB^3H_4 to a solution containing homogenous rat testis MIP synthase, G6P, and NAD, 2-inosose 1-phosphate was trapped as a mixture of tritiated *myo*-inositol and *scyllo*-inositol[106]. Iditol and glucitol, epimeric alditols representing 5-keto-D-glucose 6-phosphonate, were not significantly labeled. Its cyclization to 2-inosose 1-phosphate occurs as soon as its formation. Its reduction to putative NADH in the enzymatic reaction must be the rate-limiting step. In the presence of apo-MIP synthase reconstituted with NADH, *myo*-2-inosose 1-phosphate is converted into *myo*-inositol 1-phosphate along with oxidation of the enzyme-bound NADH.

In terms of kinetic isotope effects, with [5-^{3}H] G6P as a substrate, an isotope effect of 0.2 to 0.48 was observed[103]. An isotope effect in the reaction of D-[6-^{3}H] G6P was also reported, suggesting that removal of the hydrogen at C-6 to be partially rate determining. No isotope effects at C-1, C-2, C-3, and C-4 were detected[101, 103-104].

When reactions were undertaken with D-[5-^{18}O] G6P in H_2O or with unlabeled substrate in $H_2{}^{18}O$ using enzyme from various sources, mass spectral analysis of the products showed no exchange of the C-5 oxygen with H_2O during the reaction[3b, 3d, 31, 50]. This result is inconsistent with the involvement of a Schiff base between an active site residue and the C-5 keto group of intermediate B (Figure 3). If a Schiff base reaction were to occur, one would expect to see an exchange between the C-5 oxygen and H_2O.

When the reaction was carried out with both D-[(6S)-6-^{3}H] G6P and D-[(6R)-6-^{3}H] G6P as substrate, Floss reported that the tritium was preferentially

removed from the pro-R position by all three enzymes purified from bovine testis, *L. longiflorum*, and *S. flavopericus*[45]. Furthermore, Floss concludes that the ring closure occurs in a retention mode at C-6 of the substrate, a finding that contradicts earlier reports but agrees with the stereochemistry determined in the *S. flavopericus* reaction and with general aldolase reactions. This idea of retention of the C-6 position on the substrate turns out to be highly controversial. Other experiments contradict the Floss results. Working with the charcoal treated partially purified rat testis and mammalian enzymes, Byun and Jenness observed an uptake of tritium in both G6P and *myo*-inositol 1-phosphate from [(4S)-4-^{3}H]-NADH[107]. No appearance of tritium in either G6P or *myo*-inositol 1-phosphate was observed when [(4R)-4-^{3}H]-NADH was used. This result led to the conclusion that hydrogen transfer involves the pro-S hydrogen of NADH. However, this experimental result is not consistent with the idea that NADH remains tightly bound to the enzyme throughout the reaction. Similarly, whether the enzyme could process an enzyme-NADH-G6P complex is still questionable.

While many experiments have been done to try and elucidate the complex mechanism employed by MIP synthase, there is no discrete chemical explanation for this transformation. Although a minimal basis is available, many questions about the enzyme's mechanism remain unchallenged. Solving the structure of the inhibitor/MIP synthase complex has aided in eliminating some of the confusion. The inhibitor/MIP structure will show that the acyclic form of the substrate binds suggesting that the repositioning of the phosphate does occur

before binding. The remaining mechanistic issues are discussed in detail in the proceeding section.

Remaining Mechanism Issues

Several issues regarding this mechanism remain controversial or speculative:

(a) *Does the enzyme bind the cyclic or acyclic form of glucose 6-phosphate? What is the anomeric configuration of the C-1 carbon of glucose 6-phosphate if the enzyme does bind the cyclic form?*

It has long been assumed that MIP synthase first binds the cyclic form of glucose 6-phosphate and subsequently catalyzes the conversion to the acyclic form within the active site because the solution equilibrium of glucose 6-phosphate favors the cyclic form with a $K_{eq} > 1 \times 10^3$. This hypothesis presents a problem however, because it is expected that phosphate interaction with the enzyme is one of the most important anchoring points not only of the substrate, but of all subsequent intermediates as well. As the inhibitor structure demonstrates, the phosphate *is* the most important anchor in the substrate binding to the enzyme. The question arises as to how the substrate rearranges itself after ring opening to obtain a conformation consistent with the cyclization step. While it is still unclear, Figure 4a shows the simplest answer, which is rotation of the phosphate and hydroxyl about the C4-C5 bond resulting in phosphate repositioning. The other alternative is the conformational rearrangement proposed by Floss, which is depicted in Figure 4b. Floss believes that if the substrate is bound as the β anomer in the conformation shown, rotation

about the C4-C5 bond can occur *without* repositioning of the phosphate moiety[45]. With this conformation, he further postulates that a single residue base in the enzyme could deprotonate the O1 and O5 oxygens in the ring opening step; deprotonate C6 during the enolization step; and finally, protonate O1 during the aldol cyclization step, because all of these proton transfers occur on the same edge of the substrate. On the other hand, inhibition studies (Frost lab) indicate that, save the inosose intermediate D, only acyclic compounds effectively inhibit the enzyme, leading to the supposition that it is actually the *acyclic* form of the substrate that binds to the enzyme[44]. This would be surprising, however, because in solution, no more than about 1% of the substrate is in the acyclic form.

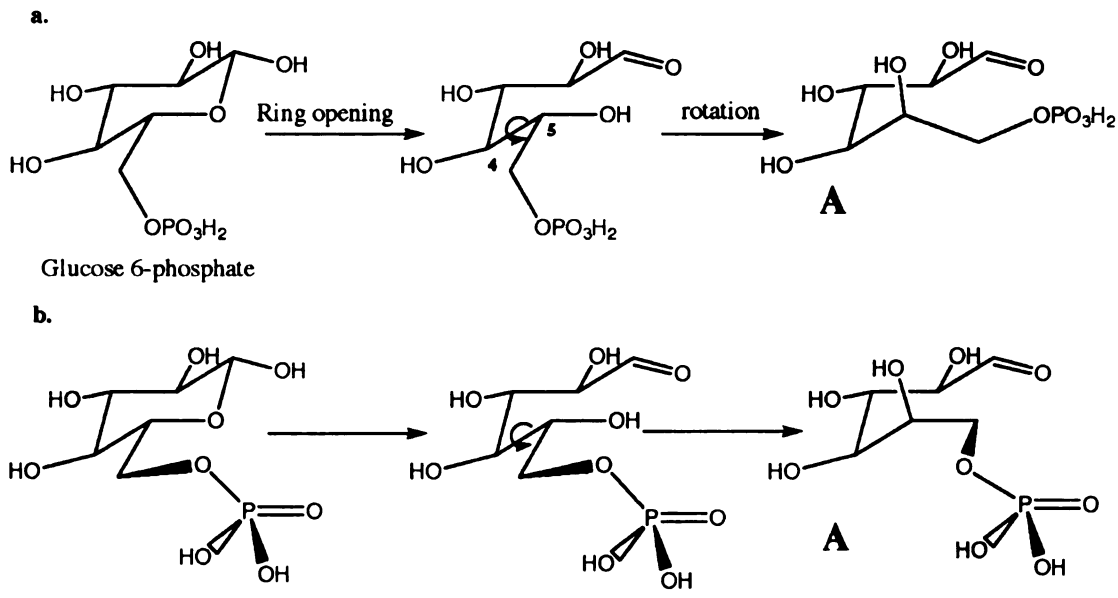

Figure 4. Two possible modes of rearrangement by the cyclic substrate. (a) The simplest rearrangement where the phosphate repositions upon ring opening. (b) An alternative rearrangement as proposed by Loewus and Floss.

(b) *What is the nature of the various proton donors and acceptors in the reaction pathway?*

While there has been much speculation regarding the role of the enzyme in various proton donation and abstraction events in the pathway, there is insufficient data to elaborate the details of this process. For example, two possibilities have been proposed for the identity of the base that abstracts the proton from intermediate B to form enolate C (Figure 3). According to Floss, a single base on the enzyme could both abstract the proton during the enol formation and then subsequently transfer the same proton to the ketone intermediate C during the aldol condensation. Similarly, this same base could also catalyze the ring opening of the glucose 6-phosphate by transferring the proton on the C1 alcohol to ether oxygen in the hemiacetal ring. Conversely, Frost and co-workers have performed inhibition studies that seem to imply that MIP synthase binds only the acyclic form of the substrate, negating the necessity for catalyzing ring opening. In addition, their studies have indicated that the phosphate group of the substrate may be the base that abstracts the proton during enol formation. The inhibitor/MIP structure complies with the Frost notion that the phosphate is the active site base that pulls off the proton during enolization and not an active site residue base.

(c) *What is the nature of the enzyme-catalyzed aldol condensation?*

Almost all enzymatically catalyzed aldol condensations utilize one of two methods for activating the aldehyde carbonyl prior to attack by the enol. Aldolases are categorized as type I or type II enzymes based on this division[46].

While type I aldolases are primarily found in higher plants and animals, type II aldolases are predominantly found in bacteria and fungi. In type I aldolases, the ketone is activated by a Schiff base formation with a lysine residue (or histidine) from the enzyme (Figure 5)[47, 48]. No metal cofactor is necessary for this activation. In type II aldolases, a metal cofactor, usually zinc, acts as a Lewis acid to stabilize the developing negative charge on the keto oxygen and can chelate the enolate to stabilize this negative charge (Figure 6)[47, 49]. Neither of these mechanisms appears to explain the intramolecular aldol condensation catalyzed by MIP synthase (i.e. the transformation from intermediate B to C in Figure 3). Though some preliminary studies seemed to indicate a Schiff base intermediate, indicative of a type I aldol condensation, $NaBH_4$ reduction failed to trap the expected intermediates, nor was there any exchange of radioactivity to the product when the reaction was run in $H_2{}^{18}O$ as would be expected with the formation of a Schiff base intermediate as discussed earlier[3c]. Since yeast MIP synthase requires no divalent metal, nor is it inhibited by high concentrations of EDTA, a type II aldol condensation pathway is also unlikely, leaving the mechanism of this important step in the reaction to be essentially not understood[3a, 31, 50]. Indeed, it is intriguing to note that MIP synthase is able to efficiently catalyze this cyclization without resorting to these forms of substrate activation. Although neither mechanism is likely, the inhibitor/MIP structure indicates that a third aldolase mechanism may be the driving force for the aldol condensation. The third mechanism, a type III aldolase, utilizes a monovalent cation as a Lewis acid to stabilize the negative charge on the keto oxygen and

can chelate the enolate to stabilize the negative charge. In the inhibitor/MIP structure, the monovalent cation ion is an ammonium ion. This makes sense since yeast MIP synthase is activated five fold by ammonium ions.

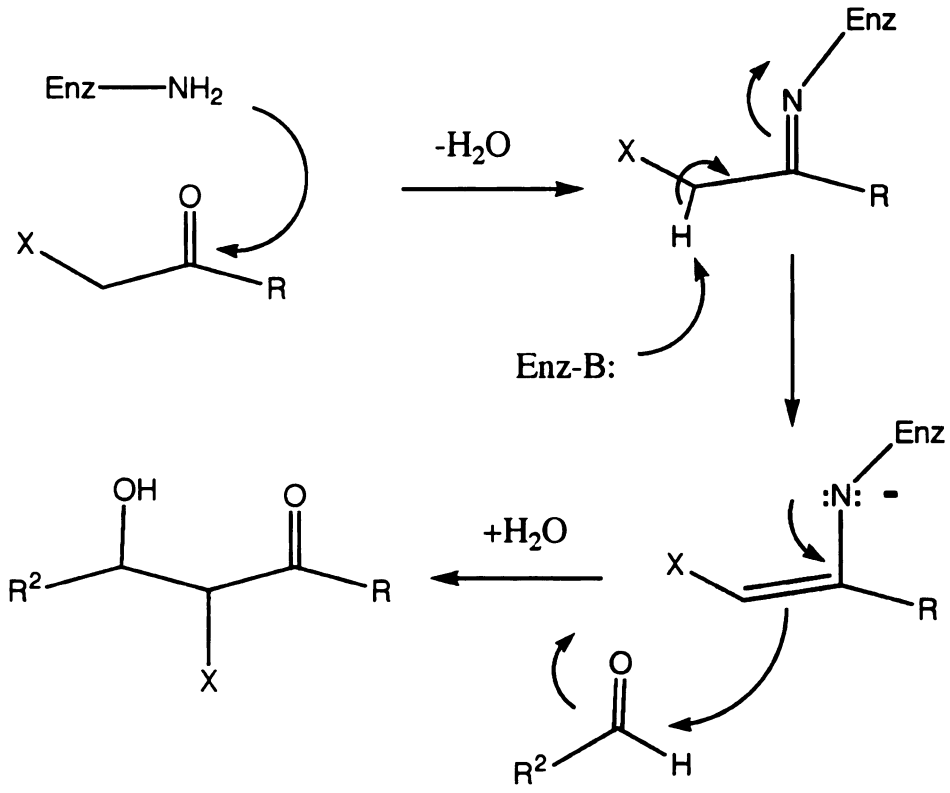

Figure 5. Schematic for a type I aldolase reaction.

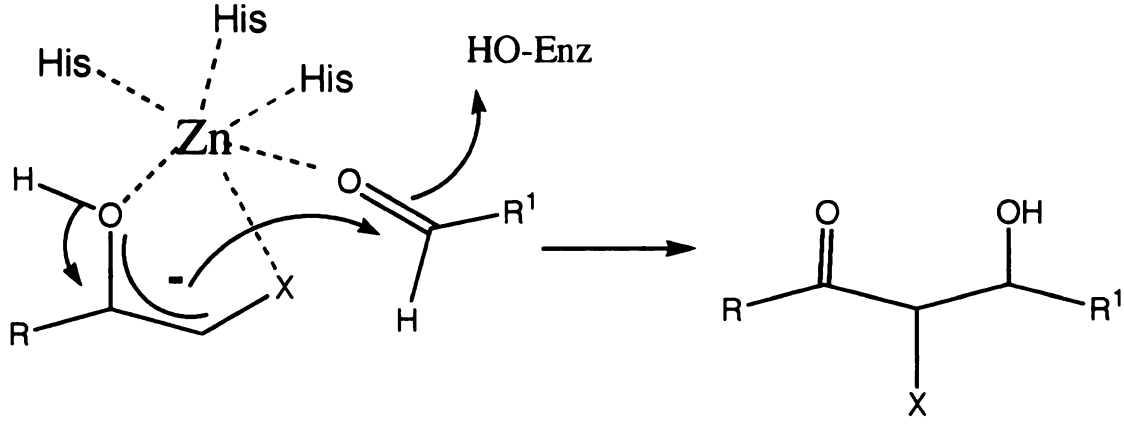

Figure 6. Schematic for a type II aldolase reaction.

(d) How does MIP synthase bind NAD?

Given the prevalence of the Rossmann-fold in most other NAD-binding proteins, it is no surprise to find that MIP synthase does contain a Rossmann fold-like domain. Though sections of the amino acid sequence of MIP synthase contain conserved glycine-rich regions, characteristic of this domain, no sequence homology can be detected between MIP synthase and any protein whose structures are known[2]. In addition, none of these glycine-rich regions matches well with the characteristic pattern of small hydrophobic and glycine residues found in these domains[51, 52]. Of additional interest, the structure of DHQ synthase has revealed an unusual interaction between the nucleotide and the Rossmann fold. This results in the active site of the enzyme being located on the opposite side of the beta sheet relative to all other known structures of this type[40]. Of all the enzymes of known structure, the reaction catalyzed by DHQ synthase is most similar to that of MIP synthase in that an oxidation, reduction, and aldol condensation all occurs in the enzyme's active site. These similarities beg the question of whether there are structural similarities in these two enzymes, particularly in the way they bind the nucleotide. Sequence alignments of the two proteins, however, reveal no homology to one another. The inhibitor/MIP structure has revealed that MIP synthase binds NAD in a fashion different from that of DHQ synthase: (1) an insertion loop in the MIP structure (residues 149-215) completely encompasses the adenine part of NAD molecule

and (2) the orientation of the nicotinamide ring is flipped 120° to that of the nicotinamide ring of DHQ synthase (see Figure 26).

AN IN DEPTH LOOK INTO PREVIOUS INHIBITOR STUDIES AND THEIR POTENTIAL ROLES IN MIP SYNTHASE CATALYSIS

An Introduction to Previous Inhibitor Studies

As stated earlier, there are several questions concerning the complex mechanism employed by MIP synthase that remain unanswered. In order to shed some light on those questions, crystallographic inhibitor studies were implemented with the hopes of developing a structural basis for the MIP synthase mechanism. The Frost group at Michigan State University were kind enough to aid in these studies with the design and synthesis of potent inhibitors that mimic most of the proposed intermediates in the catalytic cycle. Additionally, inhibitors were designed to answer specific questions regarding the enzyme's role in catalysis. The major outstanding questions regarding the mechanism of MIP synthase, as mentioned earlier in the introduction, will be further investigated here by describing the role(s) of the proposed inhibitor/enzyme complexes.

Does the Enzyme Bind the Cyclic of Acyclic Form of Glucose 6-phosphate? What is the Anomeric Configuration of the C1 carbon if the Enzyme Does Bind the Cyclic Form?

If MIP synthase first binds the cyclic form of glucose 6-phosphate and subsequently catalyzes ring opening to the acyclic form to produce intermediate A in Figure 3, the most likely mechanism for this conformational rearrangement is that depicted in Figure 4b involving rotation about the C4-C5 bond without

significant repositioning of the phosphate group. If this is the case, inhibitors that mimic intermediate A should be bound in an unique conformation with the phosphate held anti to the C5-C6 bond as shown in Figure 4b. Such acyclic inhibitors were available, either commercially or via the collaboration with the Frost group. Figure 7 shows this series of inhibitors and their K_Is[56, 72-74]. Note that all of these molecules are inhibitors because they lack an aldehyde at the terminal carbon, and are therefore incapable of undergoing the aldol cyclization. Additionally, it is interesting to note that removal of the hydroxyl group at the C2 position improves inhibition significantly. Since the substrate obviously has a hydroxyl group at this position, the reason for this improvement is completely unclear.

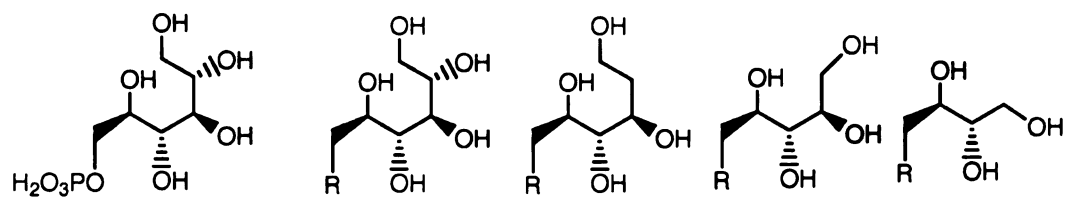

Figure 7. Acyclic substrate analogs with inhibition constants (K_I) shown below each compound.

To test whether MIP synthase binds the cyclic form of the substrate, a series of molecules designed to mimic the cyclic form of the substrate, but unable to undergo ring-opening, were synthesized (Figure 8) and all were found to be

ineffective inhibitors towards MIP synthase. This led to the supposition that in fact, MIP synthase binds only the *acyclic* form of the substrate, negating the requirement for the unique conformation described earlier.

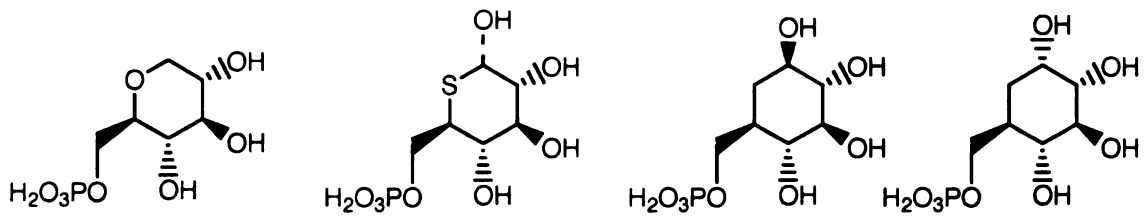

Figure 8. A series of cyclic compounds, all inactive towards MIP synthase.

To further test this hypothesis, a series of molecules were designed and synthesized, that restrict the position of the phosphate group relative to the rest of the molecule[72, 73]. This was done by replacing the phosphate moiety with a phosphonate group and introducing either a *cis*- or *trans*- double bound between the phosphonate and the rest of the molecule (Figure 9). For reference, a phosphonate is identical to a phosphate save for the replacement of the ether linkage with a methylene. According to the cyclic substrate-binding model, the *Z*-series inhibitors should more accurately mimic the structure of the acyclic intermediate in the active site. However, it is only the *E*-series of compounds that inhibit MIP synthase. As proof that these inhibitors accurately mimic true enzymatic intermediates, it was shown that these inhibitors are oxidized to the ketone by the enzymes depicted in Figure 9. Structures of one or more of these inhibitor/enzyme complexes and comparison with the above proposed structures would further verify that they undergo substrate-like binding to the enzyme. Since

they are oxidized in the active site, these structures should mimic the binding of intermediate B in the active site.

What is the Nature of the Various Proton Donors and Acceptors in the Reaction Pathway?

The combination of the above-proposed structures would be extremely informative in delineating the side chains of the enzyme that are involved in various protonations and deprotonations that occur during the catalytic cycle. The combination of a wide variety of enzyme/inhibitor structures, all of which are based on mechanistic assumptions regarding the enzyme, should add considerable weight to these assignments. The *E*-phosphonate series should be especially informative in determining whether it is the substrate phosphate or the enzyme that provides the catalyst for removal of the proton necessary for formation of the enol intermediate C (Figure 3). At present, the phosphate base hypothesis is based solely on the fact that the *E*-phosphonate series of inhibitors may indicate that the phosphate is positioned correctly to be the agent responsible for this abstraction (Figure 9). This, as described in the dgtolP/MIP synthase complex structure section, turns out to be not a hypothesis, but a structural fact.

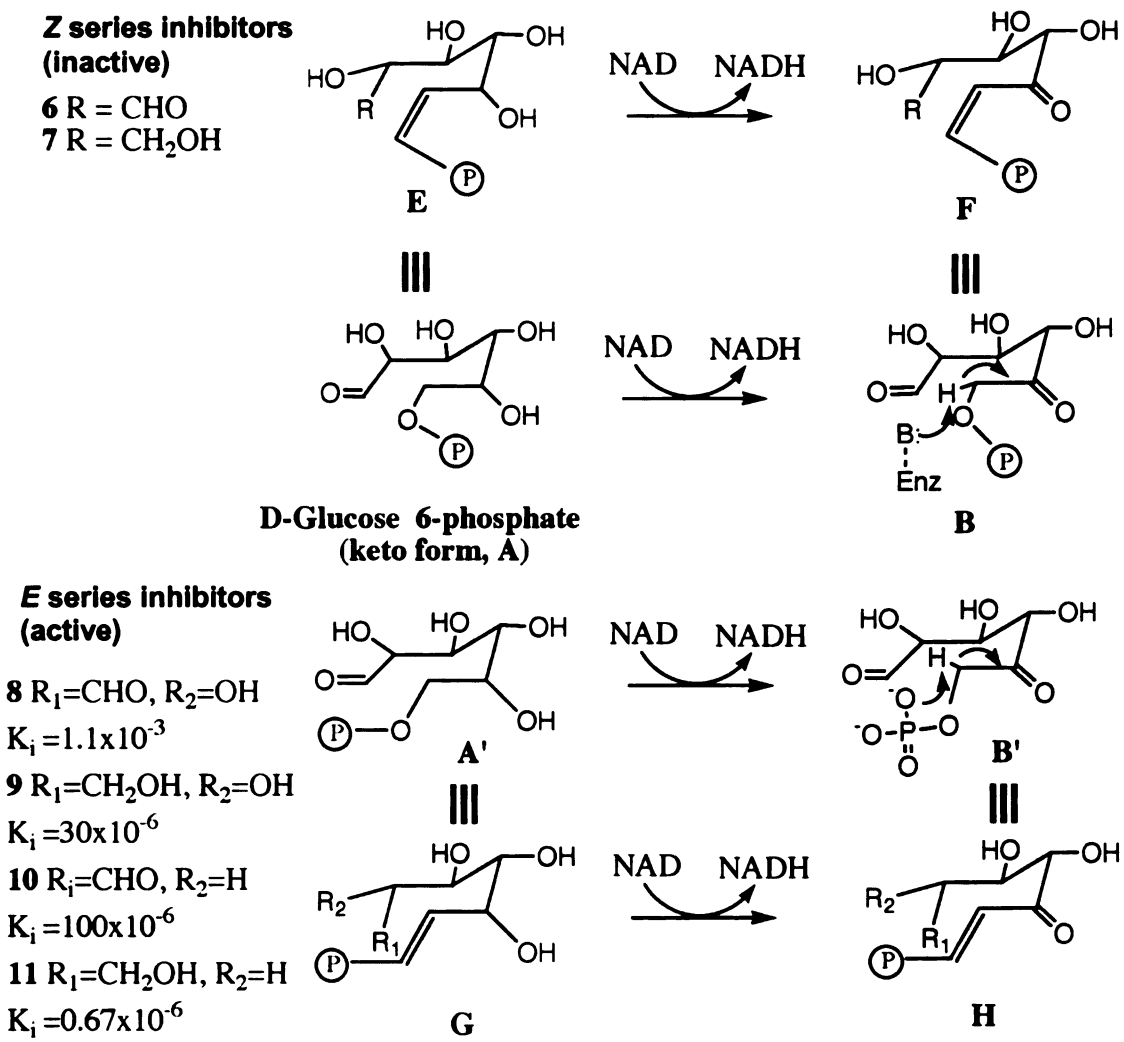

Figure 9. *E* and *Z* series of vinyl homophosphonate inhibitors. A and B are the corresponding intermediates in Figure 3.

What is the Nature of the Enzyme-catalyzed Aldol Cyclization?

As explained earlier, the nature of the aldol cyclization catalyzed by this enzyme remains mysterious as it appears to employ neither of the two well-known aldol mechanisms found in enzymes but rather a type III aldolase mechanism. The issues in this step include the following:

1. How does the enzyme orient the two ends of the molecule to optimize cyclization?
2. How does the enzyme activate the aldehyde sufficiently for aldol condensation without the use of metal cofactors?
3. How does the enzyme's active site optimally shift the keto-enol equilibrium to favor the enol form necessary for the condensation?

The mechanism of this condensation should be effectively attacked because there is significant access to inhibitors that mimic intermediates that are on both sides of the aldol condensation. The inhibitors described above (compounds 1, 2, 3, and 4 in Figure 7; compounds 9, 10, and 11 in Figure 9) together effectively mimic the intermediates (A, B, and C in Figure 3) that occur before the aldol condensation. From these structures, a general understanding of the structural details of how the acyclic intermediates are bound in the active site should be evident. Compound 10 could be especially interesting because it is the only inhibitor of MIP synthase that contains an aldehyde at C1, representing the electrophile in the aldol reaction. Additionally, intermediate D, *myo*-2-inosose 1-phosphate, has also been synthesized and found to be an effective inhibitor (K_I = 3.6×10^{-6} M)[44]. This molecule is an inhibitor because it binds the NAD form of the enzyme and therefore cannot be reduced to the final product in the active site. In summary, Figure 10 juxtaposes tight-binding inhibitors of MIP synthase with most of the intermediates in the catalytic cycle, displaying a structural map in

developing answers to many of the outstanding questions concerning the mechanism of MIP synthase.

How Does MIP Synthase Bind NAD?

As previously described, treatment of MIP synthase with activated charcoal followed by introduction of NADH is known to give the NADH form of the enzyme. This form of the enzyme should also be crystallized to elucidate the structural transformations incurred upon reduction of the cofactor. The inability of the NAD form of MIP synthase to release bound *myo*-inosose 1-phosphate (intermediate D) from the active site has led to the hypothesis that a significant conformational change may indeed occur upon reduction of the cofactor NAD to NADH. This conformational change would then result in the release of the final product MIP. These structures would give clear answers to the questions regarding the nature of the enzyme's association with its cofactor and elucidate the details of the proposed conformational change.

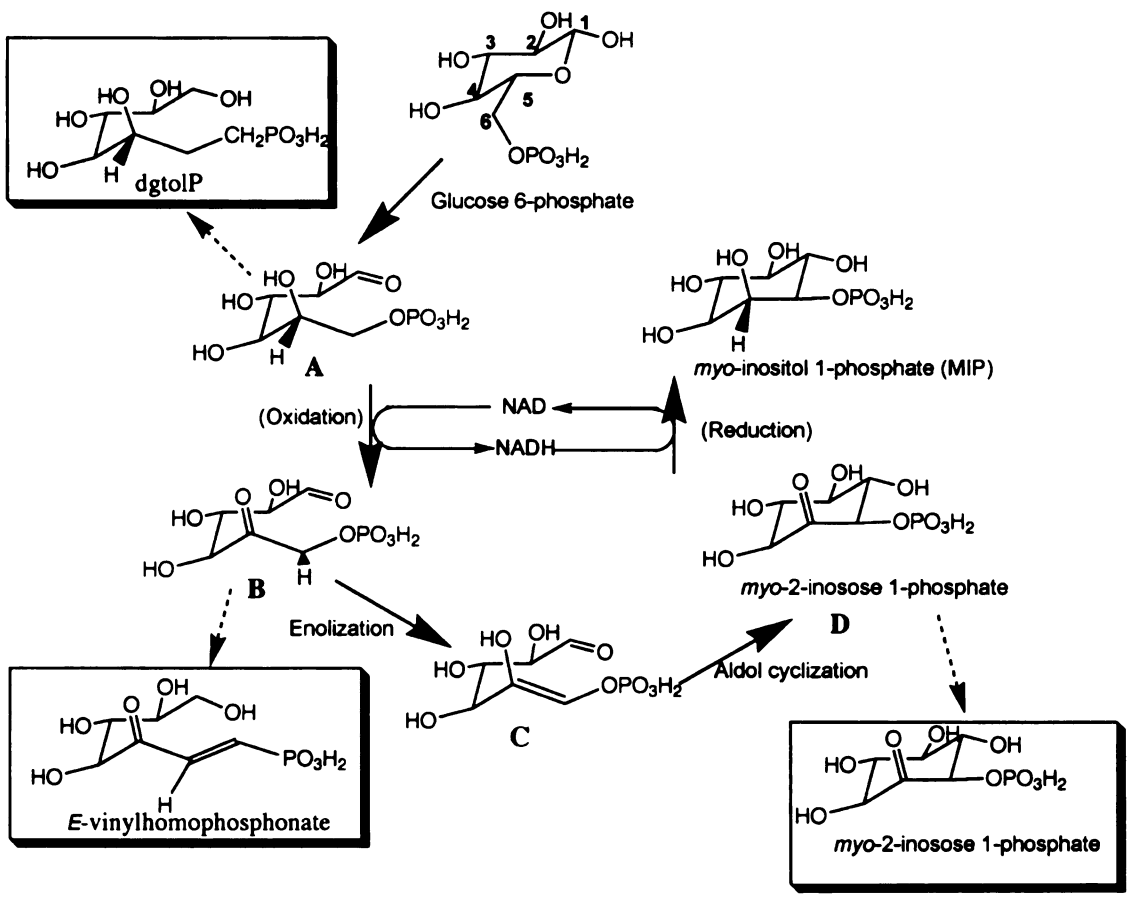

Figure 10. Mechanism and inhibitors of MIP synthase. Arrows point from proposed intermediate to active enzyme inhibitors.

GOAL OF THIS THESIS

Due to the lack of structural data, the structure of yeast MIP synthase was solved via x-ray crystallography. Similarly, to shed light on some of the mechanism inconsistencies, an inhibitor/MIP synthase structure was also solved. The purification, crystallization, structure determination, and structural results of both of these structures will be discussed in this thesis.

CHAPTER 2

THE NATIVE MIP SYNTHASE STRUCTURE

EXPERIMENTAL

Crystallization and Data Collection Analysis for the Native MIP Synthase

Two crystal forms were grown from hanging drops, via the vapor-diffusion technique at room temperature[57]. The drops were prepared by mixing 2 μL of protein solution (10 mg mL^{-1} in buffer A) with 2 μL of reservoir solution. The drops were equilibrated against 1 mL of reservoir solution. For crystallization of crystal form I, MIP synthase was equilibrated against a reservoir solution containing 2-5% (v/v) PEG 8000 and 100 mM sodium acetate (NaAc) pH 4.5. For crystal form II MIP synthase was again equilibrated against a reservoir solution containing 5-8% (v/v) PEG 8000 and 100 mM NaAc pH 5.0-6.0. Crystals from both forms were observed in 1-2 days.

For data collection, both forms can be transferred to cryoprotectant mother liquors (5% PEG 8000, 100mM NaAc at pH 4.5 or pH 5.0 depending on crystal form and 30% glycerol). Complete data sets were collected at –150°C (123K) from a single, flash frozen crystal of each form.

Native data were collected at home on an R-AXIS IIc imaging-plate system with Cu Kα x-rays generated with a Rigaku RU200 rotating-anode generator operated at 50 kV and 100 mA. Data reduction and scaling were performed using DENZO and SCALEPACK, respectively[58].

X-ray diffraction quality crystals of MIP synthase were generated using the outlined conditions. Form I crystals grew to dimensions of 0.2 x 0.4 x 0.7 mm (Figure 11a). Form II crystals have typical dimensions of 0.1 x 0.3 x 0.6 mm (Figure 11b). Since spontaneous nucleation of both crystal forms was difficult, a microseeding protocol was developed for the form I crystals that consistently yields large, single, and well-diffracting crystals. In microseeding, 2-3 crystals from a previous crystallization were crushed in a 10 μL drop of a mother liquor (5% PEG 8000, 100 mM NaAc pH 4.5). These crushed crystals were then diluted in the mother liquor in a series ranging from 10^{-3} to 10^{-7}. The ideal dilution range for yielding the aforementioned crystals was $10^{-5.5}$ to $10^{-6.5}$. Consequently, the microseeded crystals were better defined morphologically with typical dimensions of 0.2 x 0.3 x 0.4 mm (Figure 11c). Crystal form I diffracted to 2.5 Å with a data set completeness of 96.7% with a R_{merge} of 6.6%. Form II crystals diffracted to 2.9 Å with a data set completeness of 99.9%. The R_{merge} of form II was 10.7%. Both crystal forms are monoclinic with form I belonging to space group C2 and form II belonging to $P2_1$. Unit-cell parameters and data statistics are given in Table 1 for the data sets collected on each form. The volume of the unit cell for the C2 form is consistent with a 120 kD dimer in the asymmetric unit and a solvent content of 51%[59]. Similarly, the volume of the unit cell for the $P2_1$ form is consistent with a 240 kD tetramer in the asymmetric unit and a solvent content of 50%[59].

Table 1. Data-collection statistics for the two crystal forms of the native MIP synthase.

	Form I†	Form II†
X-ray Source	Rigaku RU200, 50 kV, 100 mA	Rigaku RU200, 50 kV, 100 mA
Space group	C2	$P2_1$
Wavelength (Å)	1.54	1.54
Unit-cell parameters		
a(Å)	153.0	94.5
b(Å)	96.6	186.2
c(Å)	122.6	86.5
β(°)	126.4	110.5
Mosaicity (°)	0.4	0.5
Resolution (Å)	40-2.5	40-2.9
Last resolution shell	2.6-2.5	2.9-2.8
Completeness (%)	96.7	99.9
Last resolution shell	98.9	100.0
R_{merge} ‡	0.066	0.107
Last resolution shell	0.28	0.52
I/σ(I)	15.1	13.0
Last resolution shell	3.6	2.7

† This data was collected at home.

‡ R_{merge} is defined as $\Sigma \, |I_h - \langle I_h \rangle| / \Sigma \, I_h$.

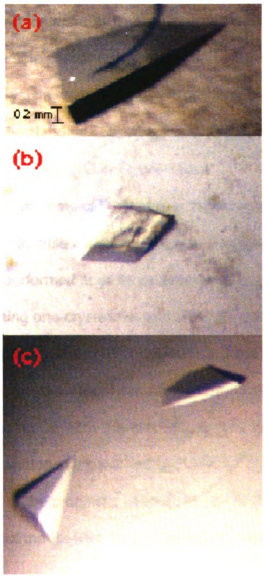

Figure 11. Crystal images. (a) MIP synthase crystal form I. Note: crystal nucleated around a fiber. (b) MIP synthase crystal of form II. (c) MIP synthase crystals produced via microseeding at a dilution of $10^{-6.5}$.

Crystallization and Data Collection Analysis of the Se-Met MIP Synthase

In crystallizing the Se-Met MIP synthase, the crystallization conditions were the same as the native protein form I. Due to the number of molecules in the asymmetric unit and the difference in diffraction resolution, the C2 space group (form I) was the sole crystal form pursued in all Se-Met structural experiments. These crystals were taken to the synchrotron to utilize the SBC-ID-19 Beamline at Argonne National Laboratory in Chicago, Illinois. The crystals described above are also depicted in Figure 11c.

At the APS, with the help of R. Zhang, a three-wavelength MAD data set was collected. In order to collect a more complete data set, a reverse beam experiment was also performed at all three wavelengths. In all, six data sets were collected (at 123K) using one crystal. As with the case of the native protein, the crystal dimensions, space group, and cryoprotectant conditions were similar. The Se-Met crystals diffracted to a little higher nominal resolution of 2.4 Å. After processing the data using DENZO, the two data sets for each wavelength were merged together and scaled using the "SCALE ANOM" command in SCALEPACK[58]. Both of the programs used were part of the HKL2000 suite package. The results of the Se-Met data collection are described in Table 2.

Table 2. Data analysis for the Se-Met MIP synthase MAD phasing experiment.

	λ_1	λ_2	λ_3
λ(Å)	0.9794	0.9796	0.9464
No. of total reflections	90,842	93,132	91,546
No. of unique reflections	49,240	49,965	49,388
Percent complete	94.1 (92.4)[a]	95.0 (93.6)	94.5 (92.6)
R_{sym} (%) [b]	4.3 (26.7)	4.7 (32.1)	4.8 (33.8)
$I/\sigma(I)$	12.7 (2.3)	14.2 (2.4)	12.6 (2.0)
Space group	C2		
Cell dimensions (Å)	a=153.00, b=96.43, c=122.66, γ=126.10°		

[a] The parentheses denote those values for the last resolution shell.

[b] $R_{sym} = \Sigma|I_o - \langle I \rangle|/I_o$, where I_o is the observed intensity and $\langle I \rangle$ is the average intensity obtained from multiple observations of symmetry related reflections.

A Primer in MAD Phasing

In solving a macromolecular structure, one needs to be able to determine the phase angle. If a protein has anomalous scatterers in its molecule, the difference in intensity between the Bijvoet pairs, $|F_h(+)|^2$ and $|F_h(-)|^2$, can be exploited to determine the phase angle. In the multiple wavelength method, the wavelength dependence of the anomalous scattering is used. Similarly, a protein should contain an element that gives a sufficiently strong anomalous signal. Therefore, the elements in the upper rows of the periodic table are not suitable. Hendrickson showed that the presence of one Se (selenium) atom in a protein of not more than approximately 150 amino acid residues is sufficient for successful applications of MAD[99]. One way to introduce Se into a protein is by growing a microorganism on a seleno-methionine (Se-Met) substrate instead of a methionine-containing substrate. Condition for application of this method is that the wavelengths are carefully chosen to optimize the difference in intensity between Bijvoet pairs and between the diffraction at the selected wavelengths[65].

Mathematically, one can describe the most frequently occurring situation where there is one type of anomalously scattering atom present. This was described by Karle in 1980[100]. In his theory, the nonanomalous scattering of all atoms in the structure is separated from the wavelength-dependent part. Each anomalously scattering atom has an atomic scattering factor of $f = f_o + \Delta f + if''$. In Figure 12, F_B is the contribution to the structure factor by the nonanomalously scattering atoms, F_A is the nonanomalous contribution of the anomalously

scattering atoms, and the complete nonanomalous part is $\mathbf{F_{BA}} = \mathbf{F_B} + \mathbf{F_A}$. The anomalous scattering contribution is:

$$\Delta f/f_o \times \mathbf{F_A} + i f''/f_o \times \mathbf{F_A} = \mathbf{a} \qquad (1)$$

ϕ_{BA} is the phase angle of $\mathbf{F_{BA}}$, ϕ_A of vector F_A, and ϕ_a of vector a. $\Delta\phi = \phi_{BA} + (180^\circ - \phi_a) = (180^\circ + (\phi_{BA} - \phi_a))$. Through mathematical manipulations, one can derive the following expression:

$$|F|^2 = |F_{BA}|^2 + p|F_A|^2 + |F_{BA}| + |F_A| \times [q\cos(\phi_{BA} - \phi_A) + r\sin(\phi_{BA} - \phi_A)] \qquad (2)$$

with

$$p = ((\Delta f)^2 + (f'')^2)/f_o^2,\ q = 2\,\Delta f/f_o, \text{ and } r = 2\,f''/f_o$$

p, *q*, and *r* are functions of the wavelength and can be derived form the atomic absorption coefficient. The $|F|^2$ values are different for Friedel mates but they can be determined experimentally. The unknown quantities are $|F_{BA}|$, $|F_A|$, and $(\phi_{BA} - \phi_A)$, all three independent of wavelength and equal for Friedel mates except for the sign of $(\phi_{BA} - \phi_A)$. Therefore, a data set at one wavelength gives two sets of equations for these three unknowns and in principle, measurements at two different wavelengths are sufficient to find $|F_{BA}|$, $|F_A|$, and $(\phi_{BA} - \phi_A)$ for each reflection. To calculate the electron density map of the protein, ϕ_{BA} is needed. This is obtained by solving the A-structure, that is by locating the anomalously scattering atoms from a Patterson map with coefficients $|F_A|^2$ or by direct methods. From the A-structure, ϕ_A can be calculated and ϕ_{BA} from the known value of $(\phi_{BA} - \phi_A)$.

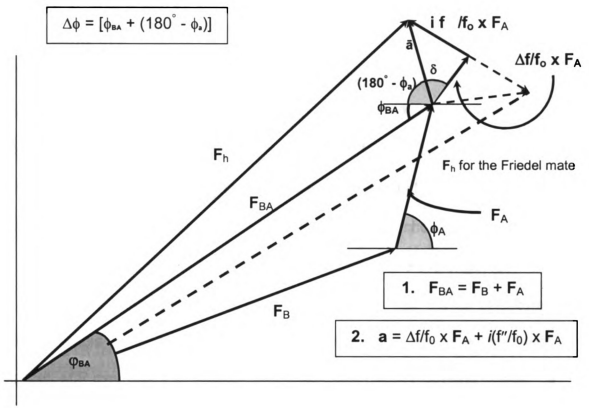

Figure 12. The structure factor diagram for the reflection of a protein crystal that contains one kind of anomalously scattering atoms. $\mathbf{F_B}$ is the contribution to the structure factor by the nonanomalously scattering atoms, $\mathbf{F_A}$ is the nonanomalous contribution of the anomalously scattering atoms, and the complete nonanomalous part is seen in equation 1. Equation 2 is the anomalous contribution of the anomalously scattering atoms. The anomalous component is exaggerated in this figure. The dotted lines are for the mirror image of the Friedel mate.

Because no anomalous scattering is taken into account for the calculation of the A-structure, the real structure or its enantiomorph is obtained. The solution of this problem is to calculate ϕ_A angles for both structures. This gives two sets of ϕ_{BA} angles and two protein electron density maps from which the best one must be selected. An advantage of this method is that nonisomorphism does not play a role here. All data can be collected on a single crystal if the lifetime of the crystal allows this.

Practically speaking, the MAD method requires that great care be exercised in the collection and processing of the x-ray diffraction intensities, because the intensity differences are rather small. The choice of wavelengths should be such that the differences between $|F(h\ k\ l)|$ and $|F(-h\ -k\ -l)|$ as well as the dispersive differences $\Delta F = <|F(\lambda_i)|> - <|F(\lambda_i)|>$ should be optimized. $<|F(\lambda_i)|>$ is the average of $|F(h\ k\ l)|$ and $|F(-h\ -k\ -l)|$ at wavelength λ_i.

Since MIP synthase can be overexpressed in *E. coli*, growth of cultures in minimal media containing Se-Met should produce protein fully substituted with Se-Met. MIP synthase's 11 methionines should give ample phasing power in a MAD experiment when converted to Se-Met. However, since both crystal forms contain more than one molecule in the asymmetric unit, the difficulty will be locating these sites in Patterson maps. In the case of the more tractable C2 crystal form, 22 sites are expected from the two molecules in the asymmetric unit.

MAD Phasing Experimental Results

After collecting and processing the three-wavelength MAD data sets, the data was then brought back to MSU and the Se-Met sites were found using the SOLVE package[63]. Through the automated search, SOLVE found 18 of the 22 sites expected from the amino acid sequence (11 per monomer and 22 per asymmetric unit). As expected, the N-terminal methionines were disordered, leaving two Se-Met sites unaccounted for. The missing sites would be defined later (non N-terminal) in the crystal structure of the inhibitor-bound complex, as these sites were located in the disordered substrate-binding domain of the structure. The final statistics for the sites found by SOLVE are tabulated in Table 3. In addition, in Table 4, the actual atomic positions are listed along with their relevant occupancies.

After finding the sites, the sites and the generated mtz file were then employed in the calculation of a solvent flattened map using the CCP4 package[64]. Subsequent maps and symmetry equivalent sites were then calculated and viewed using the TURBO-FRODO and O graphics programs[66].

Table 3. Statistics for the Se-Met sites found by SOLVE.

$$M = FOM = |F(h\ k\ l)_{best}| \ / \ |F(h\ k\ l)|^{65}$$

Figure of Merit with Resolution (FOM)

DMIN:	**TOTAL**	**8.52**	**5.54**	**4.38**	**3.74**	**3.31**	**3.00**	**2.77**	**2.58**
N:	43525	2192	3746	4810	5662	6335	6758	7039	6983
MEAN FOM:	0.60	0.84	0.86	0.80	0.77	0.69	0.55	0.41	0.29

Table 4. Se-met atomic coordinates and occupancies for the sites found by SOLVE.

Site	X	Y	Z	Occupancy	Height/σ
1	0.391	0.999	0.210	0.877	20.0
2	0.305	0.034	0.289	0.725	19.8
3	0.897	0.315	0.116	0.765	16.4
4	0.745	0.400	0.380	1.002	15.6
5	0.217	0.223	0.184	0.802	17.5
6	0.984	0.299	0.289	0.837	19.3
7	0.259	0.223	0.349	0.705	17.6
8	0.277	0.163	0.171	0.775	16.6
9	0.251	0.182	0.133	0.502	15.0
10	0.006	0.334	0.288	0.890	15.2
11	0.235	0.192	0.335	0.896	15.3
12	0.190	0.227	0.286	0.684	11.4
13	0.014	0.297	0.249	0.693	14.8
14	0.816	0.366	0.041	0.609	15.1
15	0.818	0.384	0.077	0.538	13.8
16	0.542	0.119	0.352	0.918	12.7
17	0.994	0.200	0.010	0.678	10.3
18	0.008	0.312	0.026	0.299	8.00

Refinement Analysis for the Native Structure

Once the 18 Se-Met sites were found, heavy atom refinement and calculation of an interpretable electron density map was performed using SOLVE. After solvent flattening, the map was then traced using O and TURBO-FRODO. Subsequently, using CNS, refinement began after tracing was completed[63]. Early rounds of refinement consisted of annealing, rigid-body calculations, simulated annealing omit maps, minimizations, and group b-factor refinements. After multiple rounds of calculations, the later rounds mainly consisted of minimizations, individual b-factor refinements, and bulk solvent corrections. Some 2-fold averaging was performed to see if any of the disordered regions were better defined. Unfortunately, 2-fold averaging did not help the quality of the maps. Similarly, $3F_o$-$2F_c$ maps were also calculated to improve the phasing of the disordered regions. Contrary to the averaged maps, these maps helped resolve 2 disordered loops in the determination of the final structure. Once the R-factor was reasonable (R/R_{free} 25% and 28%, respectively), waters were then added using both the CNS and TURBO packages. The final model at 2.4 Å has an R and R_{free} of 20.5% and 24.3% respectively. The final model contains residues 10-351 and 410-533 for both molecules in the asymmetric unit and 543 water molecules. All but 6 (1.1%) residues lie within the most favored or allowed regions of the Ramachandran plot. The parameters evaluated by PROCHECK were well within the bounds established from well-refined structures at the equivalent resolution[68]. The final refinement statistics are shown in Table 5.

Table 5. Refinement statistics for the native MIP synthase structure.

Refinement[a]	
Resolution range (Å)	10.0-2.4
R/R_{free} (%)[b]	20.5/24.3
Number of waters	543
R.M.S. Deviation	
Bond angles (°)	1.9270
Bond lengths (Å)	0.0095
Average B-factor (protein) ($Å^2$)	24.3

[a] Data collected at the SBC ID-19 beamline at Argonne National Laboratory.

[b] $R = \{\Sigma||F_{obs}| - |F_{calc}||/\Sigma|F_{obs}|\}$ and $R_{free} = \{\Sigma||F_{obs}| - |F_{calc}||/\Sigma|F_{obs}|\}$, where all reflections belong to a test set of 10% randomly selected data. Also, all refinement statistics were calculated with a 2σ cutoff.

STRUCTURAL RESULTS AND DISCUSSION

The Structure of the MIP Synthase Tetramer

MIP synthase is a homotetramer both in solution and in the solid state (Figure 13)[2, 56]. As shown in Figure 13, the tetramer has 222 symmetry with a non-crystallographic two-fold axis relating the two molecules in the asymmetric unit and a crystallographic two fold axis relating the two molecules at the top of Figure 13 (the red and blue monomers) with those at the bottom (the two green monomers). The interface between the non-crystallographic dimer (the dimerization interface) is both large and intricate, burying 11,700 $Å^2$ of surface area between the two. Interactions are made throughout the molecule, from the top of the structure to the bottom. The surface is composed mostly of hydrophobic residues making it unlikely that there is any dissociation of the tetramer. The interactions along the tetramer interface are listed in Table 6.

The Structure of the MIP Synthase Dimer

Though not as involved as the dimerization interface, the interface between the dimers is also significant, burying around 6,000 $Å^2$ of surface area. A front view of the dimer is shown in Figure 14. All the interactions in this interface emanate from the juxtaposition of two large beta sheets, one from each dimer. Most of the interactions among the dimer interface are hydrophobic in nature with some tight salt bridges. All of the dimer interactions are listed in Table 7.

Table 6. Native MIP synthase tetramer interactions.

Q95A----------Y166B	Q95B----------Y166A
K97A----------L164B	K97B----------L164A
E98A<-------->Q126B	E98B<-------->Q162A
Q162A---------K97B	Q162B---------K97A
E165A<------->K98B	E165B<-------->K98A
Y166A---------Q95A	Y166B---------Q95B
Y349A<------->Y349A	Y349B<-------->Y349B
M415A---------Y349A	M415B----------Y349B
E417A<------->Y349A	E417B<-------->Y349B
H433A<------->E417A	H433B<-------->E417B

<-------> Indicates a hydrogen bond interaction

---------- Indicates a hydrophobic interaction

Table 7. Native MIP synthase dimer interactions.

S11A<-------->R44B	K101A<-------->E421B	I341A----------G107B
V12A --------- F45B	F106A --------- L422B	L422A----------L440B
K13A<-------->D46B	G107A -------- A339B	L422A----------F106B
V14A -------- V47B	S113A<-------->D338B	M423A<-------->T443B
V15A -------- V47B	L117A --------- F45B	M423A<-------->S84B
Y32A<-------->E529B	L117A --------- V47B	L424A----------F94B
E33A<-------->K18B	G118A ---------A35B	L424A----------L164B
N34A<-------->E529B	G118A ---------V37B	L424A----------P103B
A35A --------- I119B	I119A ----------V36B	G425A----------F94B
V36A --------- I119B	I119A ----------V37B	G425A----------L440B
V37A --------- G118B	N124A<-------->H498B	H427A<-------->E98B
V37A --------- V126B	V126A --------- V37B	N428A<-------->N434B
R44A<-------->S11B	A128A --------- F45B	R429A<-------->H433B
F45A --------- V12B	L164A --------- L424B	R429A<-------->N434B
D46A<-------->K13B	L328A --------- F335B	R429A <-------->V435B
V47A -------- V14B	V331A -------- F335B	S431A <-------->H433B
V47A -------- L117B	L332A --------- L328B	I431A----------I432B
V47A -------- V15B	F335A --------- L328B	H433A<--------->S431B
P49A -------- V15B	D338A<-------->R507B	N434A<--------->R429B

<----------> Indicates a hydrogen bond interaction

---------- Indicates a hydrophobic interaction

Table 7 (cont'd)

F56A----------F528B	A339A--------G107B	V435A<------->R428B
F94A----------L424B	G340A--------F106B	C436A<------->H427B
C436A<------->N428B	L503A----------F335B	N524A<------->Y30B
L440A----------L422B	N504A<------->N504B	E525A<------->K505B
L440A----------G426B	K505A<------->E525B	L526A----------F513B
T443A<------->M423B	R507A<------->D338B	K527A<------->Y32B
F477A----------L532B	T508A----------E525B	F528A----------F56B
Y478A<------->R531B	N512A<------->N524B	E529A<------->Y32B
T482A<------->E530B	F513A----------L526B	E530A<------->R494B
T482A<------->R531B	F513A----------L526B	R531A<------->T482B
R494A<------->E530B	L520A----------V47B	
H498A<------->N124B	S522A<------->S522B	

<----------> Indicates a hydrogen bond interaction

---------- Indicates a hydrophobic interaction

The Structure of the MIP Synthase Monomer

The MIP synthase monomer can be divided into three major domains, each with its own distinct function (Figure 15). A central domain consisting of the N- and C-termini make the majority of contacts between monomers across the non-crystallographic two-fold and stabilize the relative orientation of the other two domains. A domain reminiscent of an NAD-binding or Rossmann fold domain (encompassing residues 66 - 326) contains a parallel five stranded beta sheet, four surrounding helices, and 2 additional extensions, one that completely surrounds the adenine of NAD preventing ready dissociation of the nucleotide (residues 149-215) and one insertion between the first and second strands of the Rossmann fold (residues 93-140) that folds into the central domain of the enzyme. The third domain (encompassing residues 327 - 441) contains the beta sheet involved in the tetramerization interface and the catalytic domain.

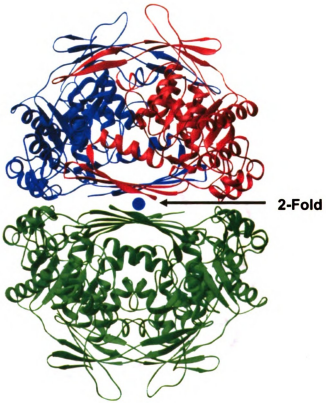

Figure 13. Ribbons model of the MIP synthase tetramer. The top two monomers are colored red and blue, make up one asymmetric unit, and are related by a non-crystallographic two-fold axis that is roughly in the plane of the page. The bottom two monomers are green and are related to the top two monomers by a crystallographic two-fold axis running roughly perpendicular to the page.

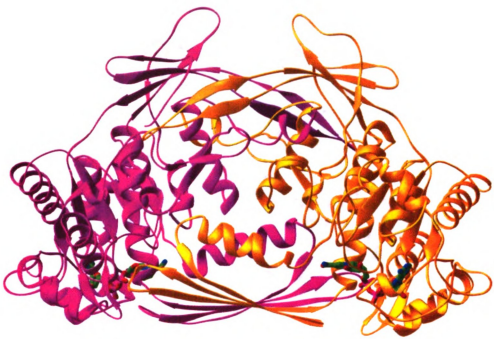

Figure 14. A front view of the native MIP synthase dimer.

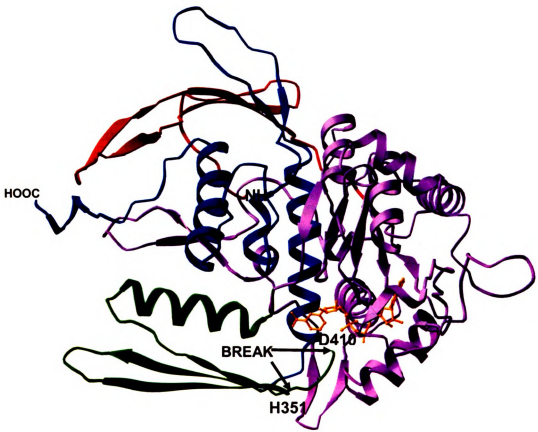

Figure 15. Ribbons model of the MIP synthase monomer. The various regions are colored: red for the N-terminal region from residue 10-65; purple for the NAD-binding domain encompassing residues 66-326; green for the catalytic or tetramerization region containing residues 327-441 (with residues 352-409 disordered); blue, the C-terminal region containing residues 442-533. Note: the N-terminal, C-terminal, and an insertion from the NAD-binding regions are intimately associated. Together, they make up the central domain of the protein.

Numerous interactions between these three domains create a rigid overall structure with little possibility for relative motion between these domains. Inspection of Figure 2 indicates that though all eukaryotic MIP synthases are highly conserved throughout their length and will almost certainly have very similar structure throughout, a significant portion of the N-terminus is missing in the archae enzyme. This will lead to differences in the structure of the central domain of this enzyme relative to that seen here. As mentioned earlier, the fold of MIP synthase bears some resemblance to that of diaminopimilate dehydrogenase (DAPDH), especially the structure and relative position of the catalytic and Rossmann fold domains[69, 70] (Figure 16). DAPDH is a dimer in solution and shares a similar dimerization interface with MIP synthase as well. Interestingly, the insertion domain (Figure 16) in DAPDH corresponds to the disordered part of the native MIP synthase structure where some of the active site residues are located.

NAD Binding

Interaction of MIP synthase with NAD is similar to that seen in other Rossmann fold NAD-binding enzymes. NAD runs across the bottom of the parallel beta sheet of the nucleotide-binding domain. Instead of the more common GXGXXG motif, MIP synthase has a GXGGXXG motif (GLGGNNG) (encompassing residues 72-78) in the loop connecting the β3 strand and α1 helix. This loop makes interactions with the phosphodiester backbone as seen in other structures. The amide of the nicotinamide is rotated to the phosphodiester

side and makes a tight hydrogen bond with the phosphodiester backbone serving to stabilize this orientation. Numerous interactions between NAD and the enzyme are observed throughout the nucleotide-binding and catalytic domains of MIP synthase. In turn, most of these residues are highly conserved amongst the eukaryotic enzymes. The nucleotide binding domains of the archaebacterial enzymes are less highly conserved and many of the interacting residues are different in these enzymes. The significance of these differences must await the structure determination of these enzymes. A complete listing of NAD-binding residues is shown in Table 8. As shown in Table 8, the differences in sequence between the archaebacterial and yeast forms of the enzyme are striking. Of the 28 interacting residues, 13 are different in the archae form (46% of the interacting residues). Interestingly, as stated in the previous section, residues 149-215 completely encapsulate the NAD and prevent it from dissociation. The residues involved in NAD-binding and encapsulation are listed in Table 9. Noticeably, there are several differences in the binding from yeast to archae. In fact, of the 9 residues, 6 are different in the archae form (67% of the interacting residues).

Table 8. Residues that bind NAD in both the yeast and archae form of MIP synthase as seen in the holo structure.

Invariant	Yeast	Archae
I71	G72 ---------->	S13
G75	G74 ---------->	T15
W147	N76 ---------->	M17
D148	N77 ---------->	V18
I149	S184 ---------->	G98
R160	N194 ---------->	S105
T244	Q195 ---------->	G106
A245	D196 ---------->	I107
T247	E197 ---------->	K108
S296	W243 ---------->	N146
P297	N246 ---------->	S149
D320	L321 ---------->	G224
K322	S323 ---------->	T226
D438		
A442		

Table 9. A list of the insertion residues that completely encapsulate the NAD in both the yeast and archae forms as seen in the holo structure.

Invariant	Yeast	Archae
I149	S184	G98
N150	I185	T99
R160	N194	S105
	Q195	G106
	D196	I107
	E197	K108

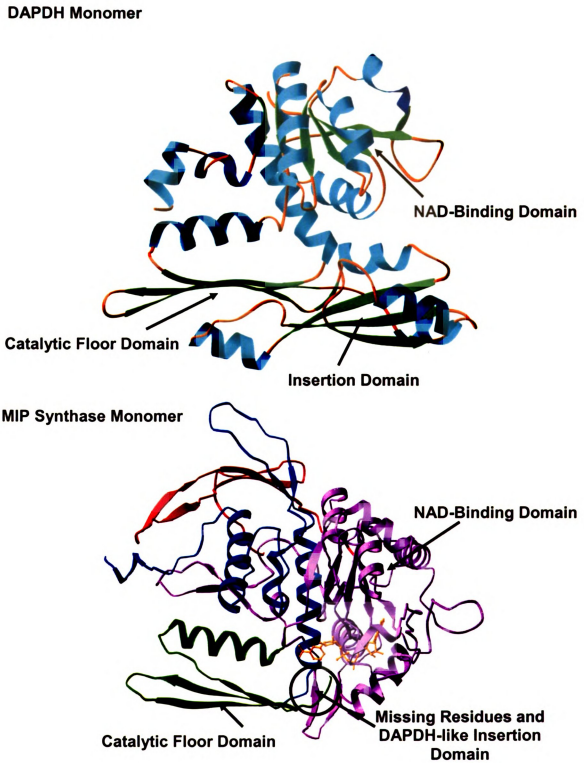

Figure 16. The DAPDH monomer (PDB accession code 1DAP) (top) in comparison to the holo MIP synthase monomer (bottom).

MIP Synthase and its Unique Rossmann Fold

Through an exhaustive search of the PDB Data Bank, a list of the various Rossmann-fold motifs was compiled. After inspection of the list, MIP synthase seems to have a unique Rossmann-fold. No other Rossmann-fold was found to have a 5,4-motif with two insertions (5 β-sheet – 4 α-helix, or more commonly, β-α-β-α-β-α-β-α-β motif). The search revealed that Rossmann-folds can be classified into three categories: 5,4-motif with one (or none) insertion, the typical 6,5-motif, and a 7,8-motif. There is no other known structure with a 5,4-motif and two insertions. The closest ancestor is the 5,4-motif with one insertion. This type of motif is seen in the enzyme aldehyde dehydrogenase (ALDH) (pdb accession code 1AD3). ALDH is interesting in that it seems to have two Rossmann-folds per monomer, even though there is only one NAD molecule per monomer. Figure 17 summarizes the results of the Rossmann-fold search.

Conclusions

The 2.4 Å structure of MIP synthase as purified from *E. coli*[71] revealed partial NAD occupancy in the NAD-binding domain and allowed us to define the catalytic region of the enzyme based on the position of the nicotinamide. Surprisingly, the nicotinamide was completely exposed on the surface of the structure with no discernable active site cleft or cavity surrounding it (Figure 18). Additionally, we were unable to locate electron density for 58 residues, from 352 - 409. These residues represent the most conserved region of the enzyme, sharing 73% identity from archae to humans. The beginning and end of this

region are located near the putative catalytic region defined by the position of the nicotinamide. In an effort to shed light on this unusual combination of observations, we grew crystals of MIP synthase in the presence of 10 mM dgtolP (Figure 3).

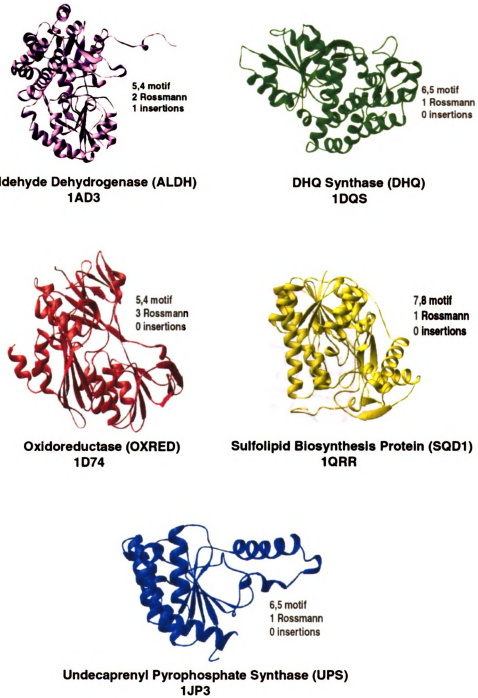

Figure 17. A thorough Rossmann-fold search results. These structures represent the types of Rossmann-folds as seen in the PDB Data Bank.

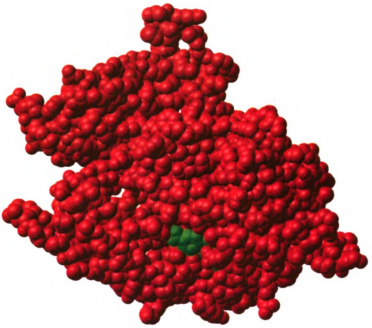

Figure 18. A space-filling model of MIP synthase in its substrate-unbound form. The protein atoms are red while the NAD atoms are green.

MATERIALS AND METHODS

Expression, Purification, and Characterization for Native MIP Synthase

After analysis of an earlier protocol for the overexpression and purification of MIP synthase, modifications to the sequence of events leading up to the formation of pure native protein were made. Included in the earlier procedure were the following: an $(NH_4)_2SO_4$ precipitation step, dialysis, a long DEAE column (10 x 30 cm, 2 L gradient), BioGel column (10 x 150 cm, 6-8 hours), and a Blue A Affinity column[44, 54]. Use of this protocol yielded 3 mg/L protein, poor protein purity, as well as time consuming. This prep was clearly not enough for a crystallographic study on the enzyme. In turn, modifications were made to both improve the purity and to increase the yield. The following protocol for overexpression and purification of native yeast MIP synthase was implemented.

Previous studies yielded the cloned and purified plasmid (pT-7-7/MIPSYN) and upon initiation of this project, the plasmid was given to us via the Frost lab at Michigan State University. Yeast MIP synthase was overexpressed in *E. coli* in the efficient BL21 (DE3) overproducing strain.

The transformation protocol was as follows: After thawing out an aliquot of BL21 (DE3) competent cells, 10 ng (1 μL) of the pT-7-7/MIPSYN plasmid was added to an eppendorf tube. After tapping this tube to mix it, the tube was then cooled on ice for 30 minutes. The cells were then heat shocked at 42°C for 90 seconds and then cooled for 2 minutes on ice. After cooling on ice, 80 μL of LB media was added and the tube was incubated at 37°C for 40 minutes. After the

incubation period, the cells were then plated onto LB/AMP plates in volumes of 20 μL and 80 μL and then incubated at 37°C overnight. Glycerol stocks of viable colonies were used initially, but stopped after further tests revealed that fresh transformations yielded more proficient cells.

MIP synthase was then expressed in LB media following a 3-hour induction with 60 mg/L of IPTG (Isopropy-β-D-thiogalactopyranoside, dioxane free). Cell pellets were re-suspended in buffer A (20 mM NH_4Cl, 10 mM Tris, 10 mM β-mercaptoethanol (BME)) in a volume proportional to 2 mL buffer A per gram of dry cells and stored at –80°C.

After thawing on ice for 30 minutes, the cells were sonicated in (3) one-minute intervals and centrifuged at 4,000 rpm for 10 minutes. The resulting supernatant was purified to homogeneity using 4 chromatography steps. (i) Phast-Q chromatography (Pharmacia): protein was eluted using a linear salt gradient (high: 300 mM NH_4Cl, 10 mM Tris, 10 mM BME, low: 20 mM NH_4Cl, 10 mM Tris, 10 mM BME). The fractions containing MIP synthase were pooled and diluted with Buffer A to lower the salt concentration. (ii) Anion-exchange chromatography: diluted fractions from (i) were applied to a SOURCE-Q column (8 mL total volume, Pharmacia) in Buffer A (20 mM NH_4Cl, 10 mM Tris, 10 mM BME, 10% glycerol). Elution with a linear gradient from Buffer A to Buffer B (1 M NH_4Cl, 10 mM Tris, 10 mM BME, 10% glycerol) gave peak fractions, which were pooled and concentrated to 2 mL for gel filtration. (iii) Gel filtration chromatography: after concentration, the protein was applied to a gel filtration column (Superdex 200 16/75, Pharmacia) and eluted in the original Buffer A

(without glycerol). MIP synthase eluted from this column as a 240 kD tetramer, consistent with previous reports[44, 54]. (iv) Blue A affinity chromatography: pooled fractions from (iii) flowed through the affinity resin to remove the residual indogenous glucose 6-phosphate dehydrogenase that co-purifies with MIP synthase. The enzyme was then concentrated to 10 mg/mL for crystallization experiments.

In concentrating MIP synthase, there were a few complications. The original prep used high-pressure Amicon filters for concentration, which yielded a loss of 50-70% of the protein. When these filters were used with the new preps, the protein precipitated out of solution. As a result, to minimize loss and to prevent precipitation, the Amicon Centriprep (Centriprep-30) and Centricon (Centricon-30) concentrators were implemented. These filters increased the final yield of protein and were less expensive. In getting the protein to 10 mg/mL, one has to be careful. The protein will fall out of solution at 20 mg/mL. This is the limit of concentration. Concentration of all steps in the purification, considered this to help reduce the loss of protein. Similarly, after each concentration, a loss of about 30-50% per run was noted.

MIP synthase was further characterized by an enzyme activity assay[44, 56]. This assay involved incubation of MIP synthase with 5 mM glucose 6-phosphate and 1 mM NAD. Aliquots were removed every two minutes, added to TCA, incubated with aqueous $NaIO_4$ for 1 hour at 37°C, and quenched with Na_2SO_3. Released inorganic phosphate was determined colorimetrically[55]. Defining one unit of activity as 1 μM of MIP per minute at 37°C per milligram of enzyme, our

number of 0.26 μM $min^{-1}mg^{-1}$ compares well with typical literature values of 0.22 μM $min^{-1}mg^{-1}$ [56]. The present purification gives as much as a three-fold improvement (from 3 mg/L to 9 mg/L) in purification over previous methods and produces enzyme of superior purity (Figure 19)[44, 56].

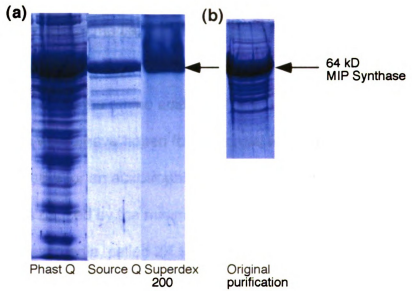

Figure 19. Purification of MIP Synthase. (a) SDS-PAGE gel of MIP synthase after each chromatographic step. (b) Purity of native MIP synthase using the previous method.

Overexpression and Purification of Se-Met MIP Synthase

In order to produce Se-Met protein, initial experiments centered on the use of minimal media (including individual amino acid supplements) as the source for culture growth[60, 61]. Unfortunately, these experiments rarely yielded functional protein (1 out of every 20 L of cell culture). All growths resulted in cell lysis presumeably attributed to the significant change in pH upon amino acid supplementation. The active range of MIP synthase in solution ranges from 7-8.4. While in minimal media, the pH was 8.4, on the high end of the range thus conceivably causing the lysis. Although some overexpression of MIP synthase was obtained using the amino acid supplement method, it was not nearly as much as one would have hoped for in a crystallographic experiment. As a result, a different media (or an auxotrophic strain) was needed to help reduce the high toxicity levels caused by the minimal media.

The new media, called 2X M9 media, was an offshoot of the often-successful minimal media. In this media, all amino acid supplements were withdrawn. As seen in Table 10, the only constituents of the media were a mixture of salts, trace vitamins, and glucose. Other additives include 100 mg/mL carbenicilin and most importantly, the Se-Met dissolved in 8M KOH. Carbenicilin was chosen over ampicilin to increase the potency of the antibiotic.

To make one liter of media, the solids were dissolved in 800 mL of ddH_2O, 20 mL of the 100X Vitamin solution (Gibco) were added, and finally, the proper amounts of the salt solutions. To bring the final volume of the media to one liter double distilled water (ddH_2O) was added. One important thing to remember is

that the vitamin solution is light sensitive so it must be protected by wrapping it in aluminum foil and storing it at 4°C.

Table 10. The make-up of the M9 media for Se-Met overexpression.

Solids	**Amount in 1L**
$(NH_4)_2SO_4$	4g
Na_2HPO_4	13.4g
KH_2PO_4	6g
NaCl	4g
Solutions	
10 mM $FeCl_3$	200 μL (autoclaved)
10 mM $ZnCl_2$	200 μL (autoclaved)
100 mM $CaCl_2$	2 mL (autoclaved)
1 M $MgSO_4$	1 mL (autoclaved)
Se-Met in 8 M KOH	100 mg dissolved in 3-4 drops of KOH
100 mg/mL Carbenicilin	1 mL (sterilize filtered)
60 mg/mL IPTG	1 mL (sterilize filtered)
100X Basal Eagle Medium Vitamin	20 mL
20 % Glucose	20 mL (autoclaved)

The overexpression of Se-Met MIP synthase is a two-day experiment and the following procedure should be implemented:

(a) Day 1 – Make all the desired media. Once this is done, autoclave the media in the following manner: Place 5 mL of culture into 10 mL test tubes, 100 mL into 250 mL flasks, and 1 L into Fernbachs. For each liter of growth, the must be one 5 mL overnight and one 100 mL secondary culture.

(b) Once all of the solutions are autoclaved, set-up the overnight cultures by taking the autoclaved 5 mL of media and add the following to it: 200 μL of 20% glucose, 200 μL of the vitamin solution, 5 μL of carbenicilin, and 2-3 colonies of MIP synthase form a fresh transformation. Grow overnight at 37°C and for at least 18 hours.
(c) Day 2 – When the overnight is a "cloudy-white" color, prepare the media for the secondary growth: To the 100 mL pre-autoclaved media, add 2 mL of 20% glucose, 2 mL of vitamin solution, and 100 μL of carbenicilin. Once these are added, take the 5 mL overnight and add the entire culture directly to the 100 mL secondary growth and grow at 37°C until an OD_{550} of 0.5-0.6. This usually takes 5-6 hours.
(d) During the intermittent period, prepare the 1 L growth: To the pre-autoclaved Fernbach, add 20 mL of 20% glucose, 20 mL of the vitamin solution, and 1 mL of the carbenicilin.
(e) When the right cell density is reached, add 50 mL culture to the 1 L of media and allow the new culture to grow until an OD_{550} of 0.5-0.6 at 37°C. This will take anywhere from 3-4 hours.
(f) At the right OD_{550},, you are ready to induce. This is the most critical step. Add to the culture 1 mL of IPTG and 100 mg of Se-Met dissolved in a few drops of 8 M KOH. Once the Se-Met is added, grow for 3 hours at 37°C. After three hours, resuspend in Buffer A and follow the same protocol for purification, as described earlier. For the Se-Met preps, DTT was substituted for BME in all buffers used in the purification. This was done to help maintain the pH of the environment. DTT is a better reducing agent.

Typical yields for the Se-Met MIP synthase prep range from 20 to 25 mg/L, a 2-fold increase from the native prep. As shown in Figure 20, a comparison between the minimal and 2X M9 growths is presented in terms of a gel. As seen in the gel, overexpression in the 2X M9 media is higher than that in the minimal media (Lane 2 as compared to Lane 3 in Figure 20). To show incorporation of the Se-Met, a mass spectrum of the substituted protein was taken by the Macromolecular Structure Facility in the Biochemistry Department at Michigan State University. From the resulting mass spectrum, the difference in weight between the Se-Met and the native MIP synthase correlates to the

amount of Se-Met incorporated. In this case, the percent incorporation was about 96%.

Modifications to the Purification Protocol as a Result of Se-Met Overexpression

In lieu of such a high yield of Se-Met protein, subsequent native preps involved the incorporation of the 2X M9 media. Instead of the typical LB media, native MIP synthase can now be overexpressed in 2X M9 media with a higher yield. Within this new expression system, a few modifications were made to the purification procedure.

The first modification involved substituting DTT for BME for the same reasons as stated in the Se-Met overexpression protocol. Similarly, the SOURCE-Q step was eliminated from the purification. Since the protein was pure enough to run over a gel filtration column after the Phast-Q column, the SOURCE-Q step was unnecessary. Finally, in the Phast-Q step, a higher gradient was used (high: 750 mM NH_4Cl, low: 20 mM NH_4Cl). The native protein in 2X M9 media seemed to bind more tightly to the Phast-Q resin, thus necessitating the increase in concentration of the high-end salt. Other than these changes, the purification protocol remained the same.

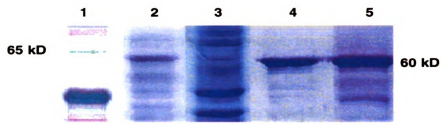

Lane 1: Kaleidescope molecular weight standard
Lane 2: 2X M9 overexpression
Lane 3: Minimal media overexpression
Lane 4: Source Q for minimal media
Lane 5: Source Q for 2X M9 media

Figure 20. A comparison between the minimal and 2X M9 media growths in the overexpression of Se-Met MIP synthase.

Multiple Isomorphous Replacement (MIR) Experimental Results

Though obtaining reproducible and well diffracting crystals of a protein or macromolecular complex is critical to solving the x-ray structure, reasonably accurate structure factor phases must also be determined to calculate an interpretable electron density map. In solving a macromolecular structure, the first method one might try is a heavy atom MIR experiment. Since reproducible and well diffracting crystals were easily obtainable, an attempt to get an isomorphous heavy atom derivative by screening a heavy atom library was made. This was pursued before any attempt in using MAD phasing to solve the native structure.

For this technique to work, most, if not all, of the protein molecules within the crystal must be identically bound by a heavy-atom-containing compound (i.e., Hg, Sm, U, etc.), with essentially no change in the structure of the crystalline lattice[62, 98]. This is usually accomplished by soaking pre-grown crystals in a wide variety of heavy atom reagents at various times and concentrations, while occasionally it is necessary to co-crystallize the protein with the heavy atom reagent.

Quite a large number of reagents have previously been used to produce satisfactory heavy atom derivatives: these include the lanthanides, actinides and uranyls, as well as mercury, gold, and platinum containing compounds[62, 98]. While uranyl acetate, the lanthanides, and actinides are considered "hard" ions that form primarily ionic interactions with proteins, the mercurials, platinates, and aurates are "soft" ions that primarily react with the sulfhydryls of cysteine

residues, the deprotonated nitrogens on histidine residues, or occasionally with the sulfur atom of a methionine residue. Since the interaction is covalent, the latter compounds tend to bind a little more specifically and are often better ordered than derivatives produced with "hard" ions.

Through an exhaustive screen, it was determined that the MIP synthase crystals were highly reactive toward all mercurial compounds tested. Concentrations of reagents as low as 1 μM crack the crystals irreversibly and severely compromise the diffraction pattern. With six cysteine residues per monomer and twelve per asymmetric unit, this is not surprising given the well-known reactivity of mercurials with sulfhydryls[62]. The most likely explanations for this behavior are: (1) one or more of the substitutions causes debilitating changes in intermolecular crystal packing interactions or (2) the rate of the substitution is too fast for otherwise acceptable and subtle lattice changes to keep up, leading to lattice destabilization and discontinuity. Table 11 summarizes the results of the most promising heavy atom derivatives obtained via soaking of the C2 crystals.

Using very low concentrations of $HgCl_2$ in ten-hour soaks significantly alters the intensity differences between native and derivatized crystals. Complete data sets on these crystals have resulted in overall intensity differences of about 20% on I when compared to the native data. Though the resulting difference Patterson maps were noisy and difficult to interpret, as many as nine unique heavy atom positions were located using the SOLVE automated heavy atom search program[63].

Unfortunately, all of these sites were of relatively low occupancy resulting in a derivative of relatively low phasing power. Though this derivative could be useful in locating heavy atoms in more complicated derivatives using the difference Fourier synthesis, it did not produce a map of sufficient quality to use in determining envelopes for noncrystallographic symmetry averaging, even after solvent flattening. These sites were found using the MLPHARE program[64]. The atomic positions and occupancies for the mercury derivative sites are described in Table 12.

Table 11. Heavy atom screening results for the most promising derivatives.

Derivative	Concentration	Time	Resolution (Å)	Deformities
p-CMB	1 mM	ON	7.0	No cracks
Mercury (II) acetate	1 mM	ON	7.0	Degraded
Mercury (II) chloride	0.2 mM	ON	3.8 wk.	Slight crack
Mercury (II) chloride	2.0 μM	ON	3.5 str.	No cracks
Samarium (II) acetate	1.0 mM	ON	No diffraction	No cracks
K_2PtCl_4	1.0 mM	ON	No diffraction	Yellow color
$KPtCl_6$	1.0 mM	ON	7.0	Yellow color
Uranium (II) acetate	1.0 mM	ON	No diffraction	Green color
$KAuCl_4$	1.0 mM	ON	No diffraction	Yellow color
$K_2Pt(CN)_4$	1.0 mM	ON	3.0	Degraded
$KAu(CN)_2$	1.0 mM	ON	No diffraction	No cracks

ON = overnight, wk. = weak, str. = strong.

Table 12. Positions and occupancies for the $HgCl_2$ derivative.

Site	Position			Occupancy	B-factor
	x	y	z		
1	0.3371	0.0017	0.0412	0.32	60.0
2	0.9488	0.1328	0.5712	0.22	15.0
3	0.9264	0.1204	0.1816	0.18	49.0
4	0.7327	0.3117	0.1141	0.22	26.0
5	0.2874	0.1507	0.4836	0.34	60.0
6	0.1043	0.0843	0.0939	0.17	57.0
7	0.2304	0.1862	0.2528	0.21	60.0
8	0.7405	0.4786	0.3737	0.31	60.0

In order to help stabilize the lattice and try to get a more isomorphous derivative, two experiments involving other heavy atoms were performed. The first involved the use of bulkier mercurials. Sometimes, more bulky heavy atom reagents will bind only to a subset of the sites that the smaller reagents bind. The types of compounds that represent the bulkier mercurials that were tested were mersalyl and phenyl mercurate derivatives. The use of the bulkier mercurials did not help in finding an isomorphous derivative. The second experiment involved controlling the rate of substitution. By gradually increasing the concentration of the heavy atom soak over a longer period of time, the rate of substitution may be more manageable. This procedure had been implemented both by gradual addition over several days and by dialysis against higher concentrations of the heavy atom derivative. Changing the rate of substitution did not improve the isomorphism necessary for a good phasing derivative. Due to poor MIR results, attempts in synthesizing a MAD phasing derivative were made.

An Attempt to Solve the $P2_1$ Crystal Form

Even though the C2 structure was solved, an attempt to solve the $P2_1$ crystal form was also made. Once it was discovered that the active site was disordered in the holo structure, interest in the enzyme turned toward solving the other form. Using AMORE in the CCP4 package, a molecular replacement solution was found[64]. Using the C2 monomer, the resulting solution contained the four anticipated molecules that make up the expected tetramer in the asymmetric unit. The correlation coefficient and the R-factor were 63.5 and 41.6%

respectively. Once the solutions were put into the right orientation using the lsqkab script, maps using the native $P2_1$ data set and the AMORE tetramer solution were calculated to 2.9 Å. Unfortunately, there were two major collisions among symmetry equivalent tetramers. Coincidentally, it was noted that there did seem to be some potential structural changes both where the collisions occurred and at the tetramer interface. In addition, partial NAD and a disordered active site also existed as previously seen in the C2 structure. Conclusively, it was decided that this crystal structure yielded no other important structural information pertaining to the existence of the active site. As a result, experiments shifted the focus on obtaining inhibitor/MIP synthase structures and no other work was done with the $P2_1$ structure.

CHAPTER 3

THE INHIBITOR/MIP SYNTHASE STRUCTURE

EXPERIMENTAL

Crystallization and Data Collection Analysis for the Inhibitor-bound MIP Synthase

In order to get a better understanding of how the complex transformations used by MIP synthase work, an inhibitor-bound protein was also crystallized. The first inhibitor used was 2-deoxy-glucitol-6-phosphate (dgtolP) due to its tight binding capability (K_I = 6x10^{-6} M) and its structural similarity to that of the acyclic form of the substrate.

The crystals of the inhibitor-bound complex were produced via co-crystallization with 20 mM NAD and 20 mM dgtolP. The crystallization conditions were similar to that of both the native and Se-Met protein. The crystal used for data collection at the SBC ID-19 Beamline (again with the help of R. Zhang) was crystallized in 3% PEG 8000 and 100mM NaAc at a pH of 4.5. Interestingly, the resolution of the inhibitor-bound complex was 0.2 Å higher than that of the native crystal. Diffraction was improved from 2.4 Å to 2.2 Å allowing for a more complete atomic understanding of the structure. This data was also processed using DENZO and scaled using SCALEPACK in the HKL2000 suite package. The crystal statistics for the dgtolP complex are described in Table 13.

Table 13. Crystal statistics for the dgtolP/NADH/MIP complex.

Resolution (Å)	2.2
No. of total reflections	76,517
Percent complete (%)	94.9 (96.3) [a]
R_{sym} (%) [b]	8.2 (30.4)
$I/\sigma(I)$	13.9 (4.6)
Space group	C2
Cell dimensions (Å)	a=152.73, b=98.31, c=121.86, γ=126.18°

[a] The parentheses denote those values for the last resolution shell.

[b] $R_{sym} = \Sigma|I_o - \langle I \rangle|/I_o$, where I_o is the observed intensity and $\langle I \rangle$ is the average intensity obtained from multiple observations of symmetry related reflections.

Solving the Inhibitor Complex and Refinement Analysis

To solve the structure of the dgtolP inhibitor complex, a difference map (F_o - F_c) was calculated using the native pdb file and the reflection file from the inhibitor complex crystal. After an initial round of refinement and calculation of a difference Fourier map using CNS, clear electron density was evident for the inhibitor, NADH, and all of the previously disordered region (residues 352-409) in a 1.2σ contoured map calculated at 2.5 Å resolution. Subsequent rounds of rebuilding, refinement, and resolution extension resulted in the final structure. The refinement rounds consisted mainly of minimizations, individual b-factor refinements, and bulk solvent corrections. The reduction of NAD to NADH and oxidation of C5 to the ketone was discernable in the electron density map. The final model contains residues 9-533, 618 water molecules, NADH, dgtolP, and one ammonium ion (per monomer). It has an R and R-free of 20.8% and 27.6% respectively. 97.8% of the entire structure lies within the most favored or allowed regions of the Ramachandran plot. The parameters evaluated by PROCHECK are well within the bounds established from well-refined structures at the equivalent resolution. Table 14 summarizes the final refinement statistics for the inhibitor-bound MIP synthase complex. Similarly, Figure 21 shows the final $2F_o$ - F_c electron density map contoured at 1.2σ near the active site.

Table 14. Refinement statistics for the dgtolP/MIP synthase structure.

Refinement[a]	
Resolution range	10.0-2.2
R/R_{free} (%)[b]	20.8/27.6
Number of waters	618
R.M.S. Deviation	
Bond angles (°)	1.7580
Bond lengths (Å)	0.0099
Average B-factor (protein) ($Å^2$)	32.2

[a] Data collected at the SBC ID-19 beamline at Argonne National Laboratory.

[b] $R = \{\Sigma||F_{obs}| - |F_{calc}||/\Sigma|F_{obs}|\}$ and $R_{free} = \{\Sigma||F_{obs}| - |F_{calc}||/\Sigma|F_{obs}|\}$, where all reflections belong to a test set of 10% randomly selected data. Also, all refinement statistics were calculated with a 2σ cutoff.

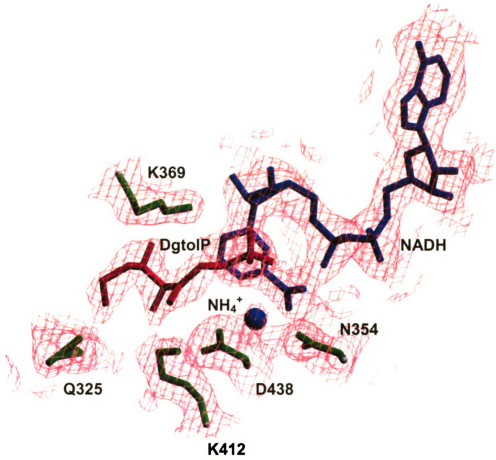

Figure 21. Final $2F_o - F_c$ electron density map contoured at 1.2σ showing the dgtolP location within the active site. The inhibitor is in red, active site residues in green, and NADH/NH_4 are in blue.

STRUCTURAL RESULTS AND DISCUSSION

The Structural Changes in MIP Synthase that Occur Upon Inhibitor Binding

The inhibitor/MIP structure yields a lot of structural information. Most importantly, the active site becomes ordered upon inhibitor binding. All of the residues in the disordered region (352-409) are clearly evident in the electron density map. These residues create an entire subdomain that folds around the inhibitor, completely encapsulating it (Figure 22). Once this subdomain is ordered, there is no access to the interior of the active site, even for a solvent molecule (Figure 23). Thus a rather large cavity is created within the structure of the enzyme. One could conclude that the formation of the MIP active site represents an extreme example of induced fit *where the substrate nucleates the folding of its own active site and its complete encapsulation within the enzyme.* Though there is little change in the structure of the rest of MIP synthase upon inhibitor binding, the loop that includes residues 191-198 is an exception, as the folding of the new catalytic domain forces this loop to flip out and create space for the newly ordered region (Figure 24). Several new contacts are made between this loop and the newly ordered subdomain as shown in Figure 24.

Similarly, several new contacts are introduced between the crystallographic dimers that make up the tetramer and the monomers that make up the dimer. These new interactions are also concentrated along the tetramerization interface as previously reported in the native structure discussion. The new tetramer and dimer interactions are listed in Table 15 and 16. Also,

listed in Table 17 are the new interactions between the resulting NADH nicotinamide ring and the new substrate-binding domain. Interestingly, 60% of the new interacting residues are different in the archae form of the enzyme.

Table 15. New tetramer interactions formed upon inhibitor binding.

N350A<------->Y349A	N350B<------->Y349B
H351A<------->Y349A	H351B<------->Y349B
D397A----------P407A	D397B----------P407B
H398A<------->M405A	H398B<------->M405B
C399A<------->M405A	C399B<------->M405B
V401A----------V401A	V401B----------V401B
K403A<-------->Y349A	K403B<-------->Y349B
M405A<------->C399A	M405B<-------->C399B
P407A----------V344A	P407B----------V344B
V408A----------Y419A	V408B----------Y419B

<----------> Indicates a hydrogen bond interaction

---------- Indicates a hydrophobic interaction

Table 16. New dimer interactions upon inhibitor binding.

S383A<------->Y127B

N384A<------->T114B

I386A----------P129B

L387A----------F106B

L392A----------F106B

<----------> Indicates a hydrogen bond interaction

---------- Indicates a hydrophobic interaction

Table 17. Additional NADH interactions in both the yeast and archae forms of MIP synthase upon inhibitor binding.

Invariant	Yeast	Archae
D356	R198	---------->E109
K369	N354	---------->D259
	N355	---------->Y260

Figure 22. Ribbons depiction of inhibitor-bound MIP synthase. The amino acids that were ordered in the holo form of the enzyme are green while the newly ordered residues (from 352-409) are red.

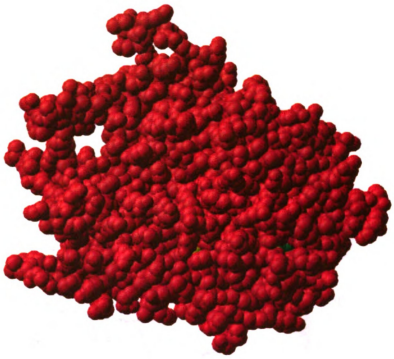

Figure 23. Space-filling model of the inhibitor-bound MIP synthase. The inhibitor dgtolP is colored yellow, NADH is green, and the protein atoms are red. Note that both dgtolP and NADH are completely obscured by the enzyme.

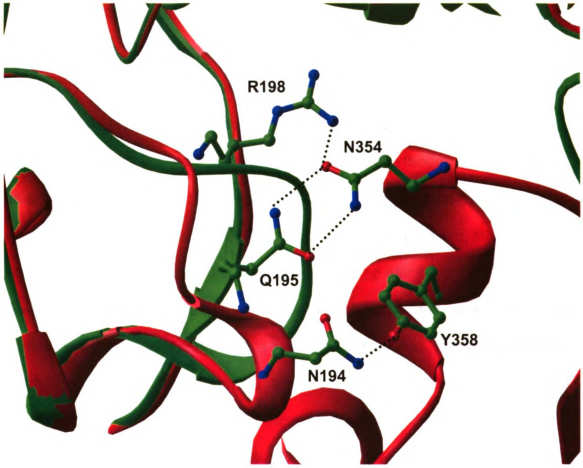

Figure 24. A view of the loop encompassing residues 191-199 that flips out upon inhibitor binding. The structures of MIP synthase bound (red ribbons) and unbound (green ribbons) by dgtolP are overlayed. Interactions between this loop and the newly formed domain are shown. Dotted lines denote hydrogen bonds. Residues are colored by atom type: green, carbon; red, oxygen, blue, nitrogen.

The Interactions Between MIP Synthase and DgtolP

The inhibitor dgtolP is bound to the enzyme in an extended conformation, with the phosphate group in a *transoid* conformation relative to the inhibitor carbon backbone (Figures 25 and 21). This conformation is consistent with several of the inhibitor studies conducted. For one, though there are many examples of exclusively acyclic substrate mimics that make good inhibitors of the enzyme, no exclusively *cyclic* mimics of the substrate bind the enzyme with any affinity[72]. As discussed earlier, the inhibitor studies suggest that MIP synthase binds exclusively the *acyclic* form of the substrate, even though the equilibrium favors the cyclic tautomer. Secondly, while 2-deoxy-D-glucitol 6-(*E*)-vinylhomophosphonate, an *E*-vinyl-phosphonate substrate mimic, strongly inhibits yeast MIP synthase, the *Z* enantiomer has no affinity for the enzyme[72]. Given these data, it is not surprising to find dgtolP bound in an acyclic, extended conformation with the phosphate in a transoid conformation. Consistent with the biochemical data, dgtolP is found to be oxidized to the C5 ketone derivative and the NAD to be reduced to NADH[72]. Evidently, we have a mimic of the first intermediate in the reaction pathway, after the first oxidation, but before enolization and intramolecular aldol cyclization.

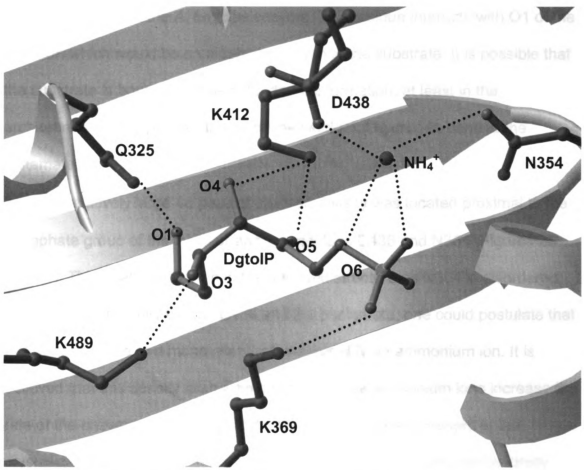

Figure 25. The interactions of dgtolP with the enzyme as seen in the structure. Dotted lines denote hydrogen bonds. Atoms are colored by atom type as in Figure 24 with the addition: magenta, phosphorous. Bonds of the inhibitor are aqua. Only residues that make direct hydrogen bonds to dgtolP are shown for clarity.

The dgtolP is well nestled in the cavity, with each of the hydroxyl groups hydrogen bonded to a highly conserved residue of MIP synthase. In fact, all but one of these residues is completely conserved in all MIP synthases. The exception is Q325, which is conserved in all eukaryotic MIP synthases, but is changed to E230 in the *A. fulgidus* enzyme. This residue interacts with O1 of the inhibitor, which would be an aldehyde oxygen in the substrate. It is possible that the substrate is bound in a less extended conformation, at least in the archaebacterial enzyme, as the aldehyde would not hydrogen bond to the glutamate.

A relatively large 4σ peak of electron density was located proximal to the phosphate group of the inhibitor and the residues D438 and N354 (Figures 25 and 21). This peak is not seen in the unbound structure as N354 is disordered. Based on its proximity to both D438 and the phosphate, one could postulate that this density is due to a monovalent cation, probably an ammonium ion. It is believed that this density is an ammonium because ammonium ions increase the rate of the enzyme five-fold. Similarly, ammonium ions are present in the crystallization solution[66]. This putative ammonium ion is roughly tetrahedrally coordinated to D438, N354, a phosphate oxygen, and O6 of the inhibitor. It is interesting to note that while D438 is absolutely conserved in all MIP synthases from archae to human, N354, while absolutely conserved in eukaryotic MIP synthases, is occupied by D259 in *A. fulgidus.* One could postulate that the addition of a second charged ligand changes the cation specificity from

monovalent to divalent, and may explain why the *A. fulgidus* MIP synthase requires a divalent cation such as Zn^{2+} or Mn^{2+} for activity.

There are two other enzymes that have both NAD and a metal ion in their active site: dehydroquinate synthase (DHQ synthase) and alcohol dehydrogenase (ADH). When the nicotinamide rings of these two enzymes are overlayed, the metal ion positions are almost identical. Further, when the nicotinamide rings of DHQ synthase and MIP synthase are overlayed, the position of the ammonium ion is within 1.0 Å of both the DHQ synthase and alcohol dehydrogenase zinc atoms (0.89 Å and 0.90 Å respectively) (Figure 26). This is in spite of the fact that none of these enzymes have any structural or sequence similarity throughout their length. Given this positional similarity, it is expected that the ammonium ion seen in MIP synthase has a role that is analogous to that seen in the other two enzymes, which is to act as a Lewis acid stabilizing negative charge on a keto oxygen atom.

DgtolP binding by MIP synthase involves both residues that were ordered in both structures and additional residues that become ordered upon inhibitor binding (Figures 25 and 2). While Q325, K412, D438, and K489 were ordered in the unbound enzyme, K369 and N354 lie within the refolded subdomain (Figure 25). Five hydrogen bonds are made between the inhibitor and the enzyme: Q325 to O1 of dgtolP, K489 to O3, K412 to O4 and O5, and K369 to a phosphate oxygen of dgtolP. The rest of the interactions are hydrophobic in nature and define a hydrophobic core of the subdomain consisting of both enzyme and inhibitor.

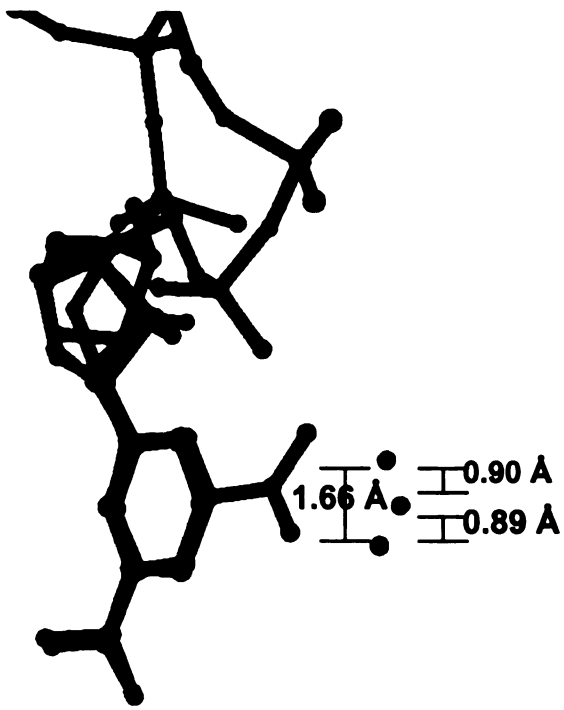

Figure 26. Overlay of the nicotinamide rings of alcohol dehydrogenase (orange), DHQ synthase (cyan), and MIP synthase (blue). The spheres represent the relative positions of the divalent metal (ADH and DHQ) and the monovalent ammonium ion of MIP synthase.

Modeling of the Aldol Cyclization and a Proposal for the Mechanism of MIP Synthase

The conformation of dgtolP in the dgtolP/MIP synthase structure is clearly not representative of the conformation of the substrate during the aldol cyclization. A simple rearrangement of dgtolP was performed in an attempt to mimic the conformation necessary for cyclization. To do this modeling, it was assumed that the phosphate and C6 remain fixed while the inhibitor was repositioned in a conformation consistent with the stereochemistry of the reaction. Additionally, the 5-keto group was oriented with the nicotinamide of NAD in a position consistent with the final reduction step. Similarly, it was assumed that the structure of the enzyme is unchanged. The result of this modeling is striking (Figure 27). Absolutely conserved residues now surround the modeled inhibitor and make hydrogen bonds with all of the OH groups. In addition, the 5-keto group is well positioned to interact with the ammonium ion and K369 is in close contact with O1 of the inhibitor. Based on this modeling, two mechanisms for the transformation catalyzed by MIP synthase can be proposed

In the first mechanism (Figure 28), the first step involves oxidation at C5 with the substrate molecule in an extended conformation similar to that seen in the inhibitor complex structure. Subsequently, the substrate is reoriented to the conformation shown in Figure 28 where the phosphate-mediated enolization occurs. The developing negative charge on O5 is stabilized by the ammonium cation to catalyze this process. Nucleophilic attack by C6 on C1 is promoted by K369 stabilization of the developing negative charge on O1. Subsequent protonation at O1, possibly mediated by K369, and reduction of C5 by NAD,

yields the 1L-*myo*-inositol 1-phosphate product. MIP synthase is therefore an example of a *type III aldolase*, where a monovalent cation acts as the Lewis acid in the aldol condensation. In the case of the archae enzyme, a similar mechanism can be envisioned, except that the ammonium ion is replaced with a zinc or manganese divalent cation, making this more characteristic of a type II aldolase. All of the other residues interacting with the substrate and proposed to be involved in the mechanism, are absolutely conserved in archae as well as virtually all other MIP synthases whose sequences are known. Given the presence of the divalent cation at this position, one would expect the residues corresponding to 350-354 (MIP synthase) in archae (255 - 259) to be ordered even in the absence of inhibitor or substrate. This would however, still leave significant access to the active site when the remainder is disordered. Verification of this proposal must await both mutational enzymology and further enzyme/inhibitor structural results.

The other possible mechanism is the scenario in which the substrate enters the active site in the alcohol form at C-5. When this occurs, the protonation is through the mediation of D438. Although the phosphate still pulls off the proton during enolization and the ammonium acts as a Lewis base stabilizing the developing negative charge on C-5, the aspartate allows the proton transfer to occur during aldol condensation. This mechanism is depicted in Figure 29.

Is the New Domain Due to NAD or Substrate Binding?

Solving the dgtolP/MIP synthase structure inevitably invokes the question of whether the presence of the new 58 residues is a result of the NAD or substrate binding. Clearly, in the presence of partial NAD occupancy, none of the substrate-binding domain residues is seen. Similarly, the loop encompassing residues 191-198 is hovering over the NAD and not flipped out making contacts with the new domain. However, what happens if there is complete NAD occupancy without the presence of substrate? To answer this question, a MIP/NAD crystal was made by soaking in 20 mM NAD into the MIP synthase crystal lattice. A data set was collected and processed to 2.7 Å. Upon calculation of a $F_o - F_c$ map, none of the substrate-binding domain residues was seen. Also, the loop that flipped out upon substrate binding, was in its native position as seen in the holo structure. Though diffusion of NAD into the lattice caused a compromise in diffraction, a well-diffracting crystal was still attainable. Conversely, co-crystallization of MIP with NAD was difficult. No crystals were obtained via co-crystallization. A more complete crystallization experiment on this complex would be beneficial to completely refute the NAD-binding argument.

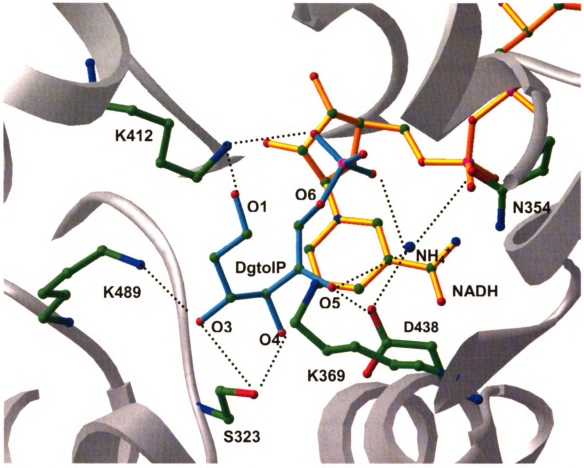

Figure 27. Modeling of dgtolP in the active site of MIP synthase to a conformation consistent with aldol cyclization and subsequent reduction at C5. Atoms are colored by atom type as in Fig. 23. DgtolP bonds are aqua and NADH bonds are gold.

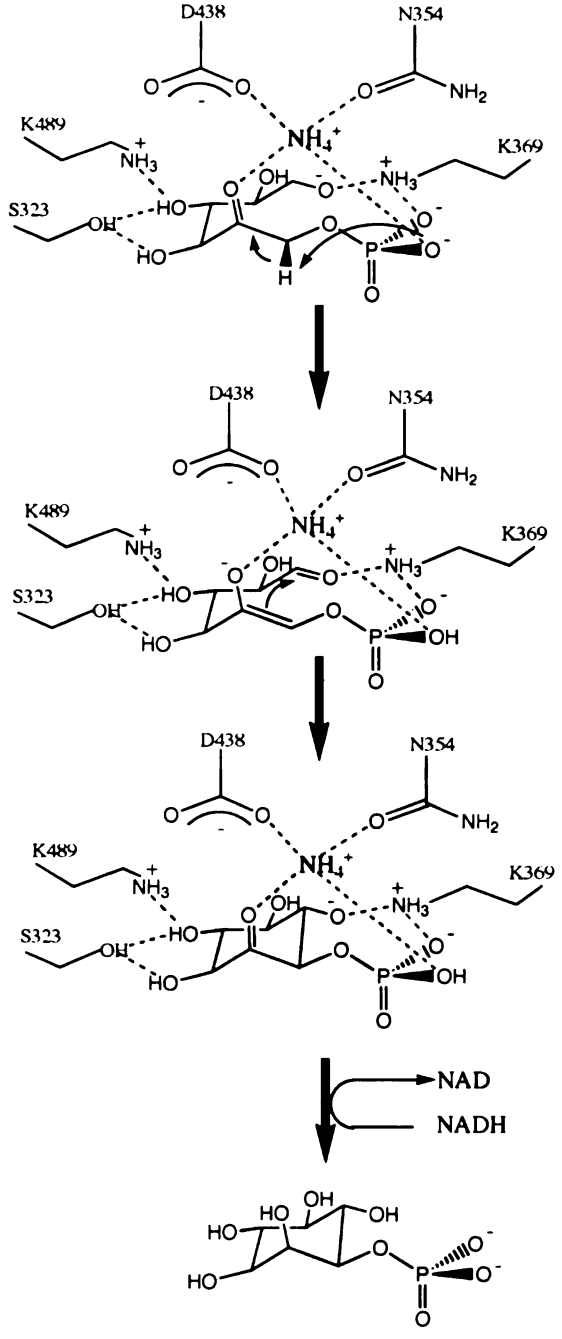

Figure 28. Proposed mechanism for the transformation catalyzed by MIP synthase.

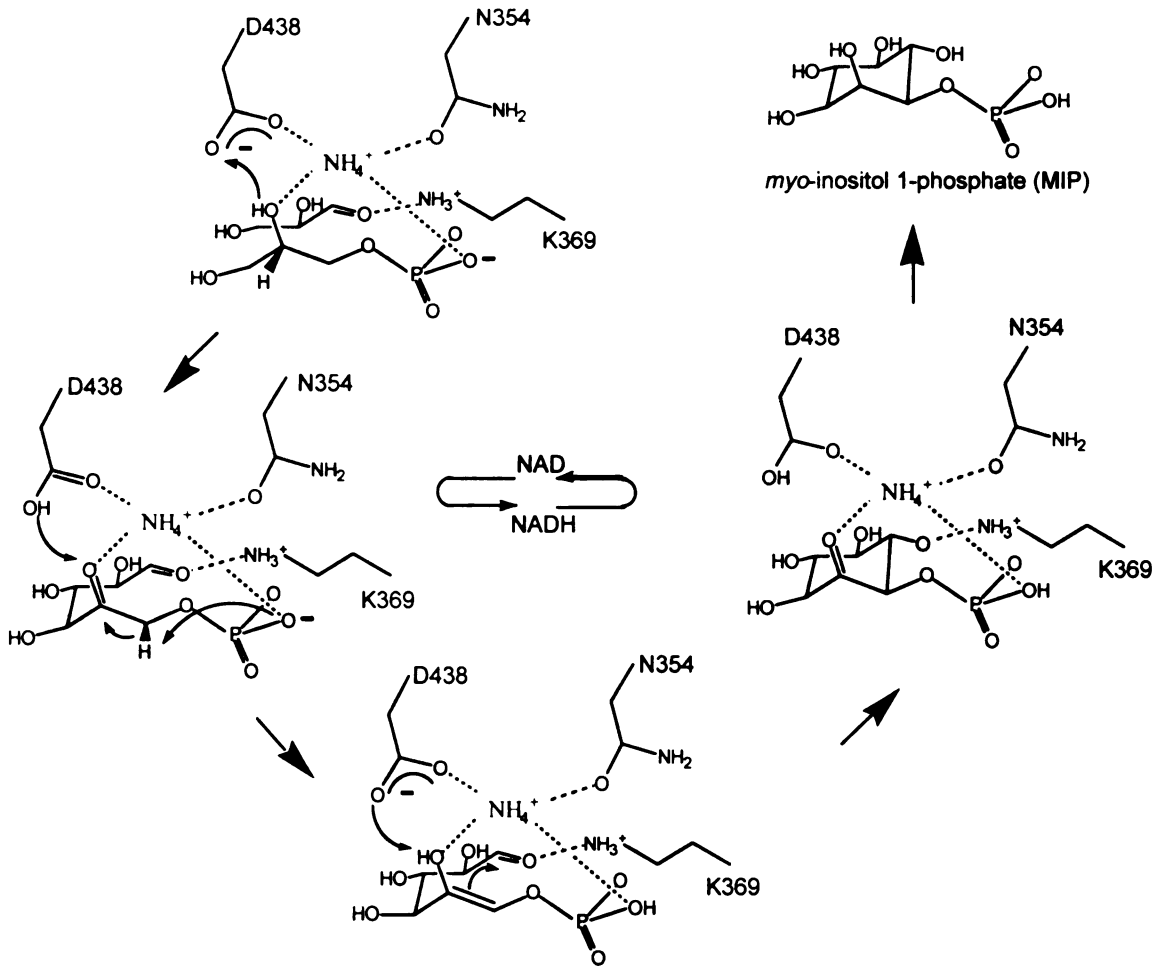

Figure 29. An alternative mechanism for the catalysis of MIP synthase.

MIP Synthase, a New Mechanism for Induced-fit?

The concept of induced-fit where "the substrate causes an appreciable change in the three dimensional relationship of the amino acids in the active site" was proposed more than 40 years ago by Koshland[75, 76]. An exhaustive search of domain movements in proteins categorizes all of these movements as either hinge movements or shear movements[77]. The structures of the NAD-bound and inhibitor/NAD-bound MIP synthase, have revealed an extraordinary example of induced-fit that complies with neither of these mechanisms. Instead, a folding event occurs where almost fifty-eight residues become ordered upon binding to the inhibitor. Once folded, the enzyme fully encapsulates its substrate, leaving no access to the active site without unfolding some or all of this subdomain. Though there are examples of ligand-induced structural organization, such as the formation of two helices upon DNA binding in the leucine zipper proteins, it is highly unusual to see a refolding event of the magnitude seen here in an enzyme with a small molecule substrate[78, 79]. This binding mechanism seems counterintuitive, but allows the enzyme to completely encapsulate its substrate in three dimensions. Encapsulation appears to be necessary for catalysis of this complex transformation. It also invites the possibility that small molecules can be used as protein folding scaffolds, both naturally and in protein engineering applications.

An Attempt in Solving Another Inhibitor Structure, the *E*-vinylhomophosphonate/MIP synthase Complex

Once the dgtolP/MIP synthase structure was solved, an attempt to solve the vinyl/MIP complex was made. The inhibitor, *E*-vinylhomophosphonate, mimics the intermediate during the enolization step of MIP synthase catalysis (Figure 10, mimic of intermediate B). A co-crystallization experiment was used (same conditions as the dgtolP/MIP complex) to generate the crystal used for data collection. After collecting data to 2.2 Å of a vinyl/MIP complex at the SBC Beamline, a difference map using the dgolP/MIP synthase pdb and the vinyl reflection file was calculated using CNS. Upon viewing the map, there was some broken density for the vinyl inhibitor. Unfortunately, something happened to the crystal during data collection, rendering a data set with non-discrete spots. As a result, the data for this crystal had to be truncated to 2.9 Å to get any value from it. This truncation severely distorted any attempt to solve this structure. Another data set of this complex was not collected again. A crystal structure of this complex would definitely absolve any question on the conformation of the substrate during the enolization and aldol condensation steps of catalysis.

CHAPTER 4

VALPROATE, A POTENTIAL THERAPEUTIC DRUG TARGET IN THE TREATMENT OF MANIC DEPRESSION

GENERAL OVERVIEW

An Introduction to Bipolar Disease

Bipolar disorder, or manic-depressive illness, is a common condition with a lifetime prevalence of 1-2%[80]. It is characterized by recurring bouts of mania and depression, which have deleterious effects on career and interpersonal relationships. Approximately 15% of those afflicted commit suicide. Others suffer with bouts of schizophrenia. Similarly, mortality rates are also increased due to physical disorders[81, 82]. For decades, lithium has been the most effective agent for the treatment of bipolar illness[83]. Despite the marked benefit that many patients obtain from lithium therapy, 20-40% of patients fail to show a satisfactory antimaniac response to lithium, and many patients suffer significant morbidity[84]. More recently, the branched fatty acid valproate has been used for treatment of bipolar disorder[85]. Like lithium, it is not completely effective, and the molecular dynamics underlying its therapeutic effects have not been elucidated. Lithium and valproate exert a variety of biochemical effects, only some of which are likely to be related to their therapeutic mechanisms of action. Identifying common targets of lithium and valproate is an approach that may more directly address the therapeutic mechanisms underlying their efficacy[86-90].

The Inositol Depletion Hypothesis

The inositol depletion hypothesis proposes that lithium acts by depletion of inositol from the brain. This is based on the observed uncompetitive inhibition of inositol monophosphatases by lithium, resulting in decreased inositol levels, an increase in inositol phosphates, and subsequent down-regulation of the phosphoinositide cycle[7c]. Because the brain obtains inositol primarily from phosphoinositide turnover and *de novo* synthesis, it is highly sensitive to fluctuations of the phosphoinositide cycle. Although there is considerable evidence that lithium affects the phosphoinositide second messenger system, a connection between this effect and the therapeutic mechanism of lithium has not been established[91-93]. If inositol depletion formed the basis for the therapeutic effect, then valproate might be expected to deplete inositol, as well. Previous studies have shown that valproate does not inhibit bovine brain or yeast inositol monophosphatase activity, nor does it have an effect on receptor-mediated phosphoinositide turnover[94-96]. Additionally, valproate does not lead to large accumulations of inositol mono- or bisphosphates, as seen with lithium[97].

Recent Data Published on Valproate Inhibition of MIP Synthase

It has been shown by Vaden *et.al.*, that both lithium and valproate have a profound effect on inositol metabolism in the eukaryote *S. cerevisae*[53]. Both drugs, in therapeutically relevant concentrations, cause a decrease in intracellular inositol mass and an increase in expression for a structural (*INO1*) and a regulatory (*INO2*) gene required for inositol synthesis. The mechanism of

inositol depletion by lithium, is most likely due to the inhibition of inositol monophosphatase, as previously reported[95]. On the other hand, the mechanism of inositol depletion by valproate is caused by the inhibition of *myo*-inositol 1-phosphate synthase[53].

Furthermore, a 40 μM inositol concentration, completely reverses the 35-fold valproate-mediated increase in *INO1* expression. Conversely, this concentration only partly reverses a smaller lithium-induced increase in *INO1*[53]. Interestingly, both lithium and valproate down-regulate the level of sodium-dependent high affinity *myo*-inositol transporter in astrocyte-like cells. The effects of these drugs on inositol uptake and transport in yeast have not been determined, although preliminary data suggests that they do not cause decreased inositol uptake[53].

In terms of a mechanism, Vaden proposes that valproate leads to decreased inositol levels by inhibition of the *myo*-inositol 1-phosphate synthase pathway[53]. Several experiments demonstrated that inositol monophosphate levels are reduced by valproate but not by lithium. Inhibition by valproate via this pathway is further supported by the observation that the *opi*1 mutant does not exhibit increased resistance to valproate, despite constitutive expression of *INO1* and increased levels of MIP synthase. Previous findings that valproate does not inhibit inositol monophosphatase or cause an accumulation of inositol phosphates has been cited as evidence against the inositol-depletion hypothesis[94, 97]. Vaden's experiments conclusively suggest the mechanism of

inositol depletion by valproate is by inhibition of the rate-limiting step in the *de novo* synthesis of inositol, via the catalysis of MIP synthase.

Other plausible mechanisms for inositol-depletion include the down-regulating expression or activity of protein kinase C (PKC)[53]. PKC is highly enriched in the brain and plays a major role in regulating, pre- and post-synaptic aspects of neurotransmission[108]. It is now know to exist as a family of closely related sub-species, has a heterogeneous distribution in the brain, and plays a major part in he regulation of neuronal excitability, neurotransmitter release, and long-term alterations in gene expression and plasticity[108]. To date, only a few studies have directly examined PKC in bipolar disorder. Although there is no evidence for PKC expression in yeast, valproate does decrease mammalian protein kinase C expression[87]. Protein kinase C appears to be required for inositol synthesis, as yeast protein kinase C mutants are inositol auxotrophs. Therefore, a valproate-mediated decrease in protein kinase C would result in decreased intracellular inositol and thus a further reduction in synthesis of inositol.

Vaden's results present one with an interesting dilemma. If valproate does inhibit the MIP synthase pathway at therapeutic levels, a potential therapeutic drug design target may have been discovered. Unfortunately, Vaden did not present any data as to the K_I value for valproate inhibition. If the K_I shows tight binding of valproate, crystallographic experiments may be warranted. Since no inhibition data was available, inhibition studies were initiated to find out what type of inhibition was present and the K_I value for valproate inhibition of MIP synthase.

Before assays were done to determine the inhibition constant, a quick glance was taken into the active site of the dgtolP/MIP synthase complex to try to determine *if* there was a potential valproate-binding site. Interestingly enough, there was an identifiable hydrophobic pocket, consistent with the chemical properties of valproate.

ASSAY RESULTS AND DISCUSSION

Potential Valproate Binding Site in MIP Synthase

Valproate (2-propyl-pentanoic acid), at least chemically, seems to mimic the structure of the glucose 6-phosphate. As seen in Figure 30, valproic acid has a negatively charged carboxcylic acid end, which could conceivably mimic the phosphate group of the glucose 6-phosphate. The other end of the molecule is highly hydrophobic consisting of a branched carbon backbone. As a result, one can envision that the presence of a highly hydrophobic pocket in the active site would serve as a viable binding site for the valproate molecule.

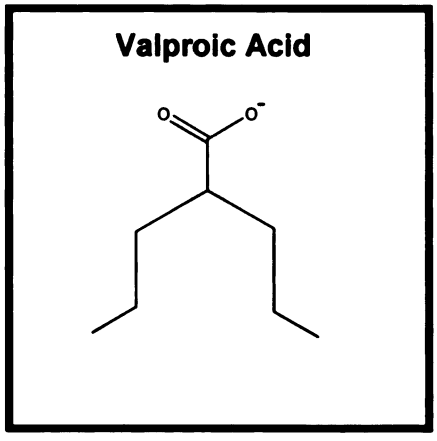

Figure 30. Chemical structure of valproic acid.

Coincidentally, a large hydrophobic surface consisting of residues L352, L360, I400, and I402 aligns one side of the binding cavity. These hydrophobic residues are completely conserved throughout evolution. Structurally, this hydrophobic pocket is depicted in Figure 31. In order to substantiate this claim

and to see if the relevant crystallization experiment was worthy, activity assays to determine the K_I for valproate inhibition were performed using the Ames colorimetric method as described earlier[55].

Assay Results

After determining the activity constants for each trial of inhibitor concentration, plots were made to determine the K_I for valproate inhibition. From these plots (Figures 32 and 33), a K_I of 0.7 mM was calculated. To determine what type of inhibition was present, a Lineweaver-Burke plot was made (Equation 3).

$$1/v = [K_m[1 + [I]/K_I]/V_{max} \times 1/[S]] + 1/V_{max} \qquad (3)$$

When 1/v was plotted against 1/S, all lines intersected at a single point with each concentration of inhibitor (Figure 32), consistent with competitive inhibition. To further verify a competitive inhibition mode, a Hanes-Woolf plot was made (equation 4). In this plot, for competitive inhibition, lines at various concentrations of inhibitor are parallel with each other. As shown in Figure 33, all lines were parallel to each other, signifying competitive inhibition.

$$[S]/v = K_m[1 + [I]/K_I]/V_{max} + 1/V_{max} \times [S] \qquad (4)$$

This technique was also tested against previous inhibition assays to determine its validity. Those experiments yielded no significant deviation from previous assays on those inhibitors with published K_I's. For example, when an inhibitor assay was done with dgtolP on MIP synthase with the technique used in the valproate inhibition assay, a K_I of 5.5 μM was calculated. This value is in agreement with the reported value of 5.8 μM by the Frost group.

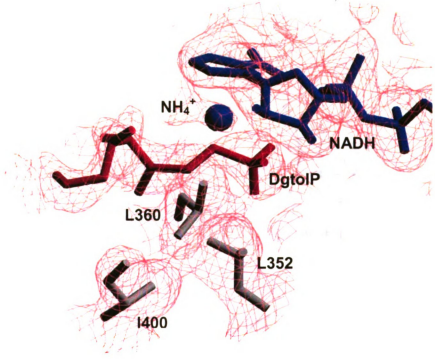

Figure 31. Potential valproate binding site. The map is contoured at 1.2σ.

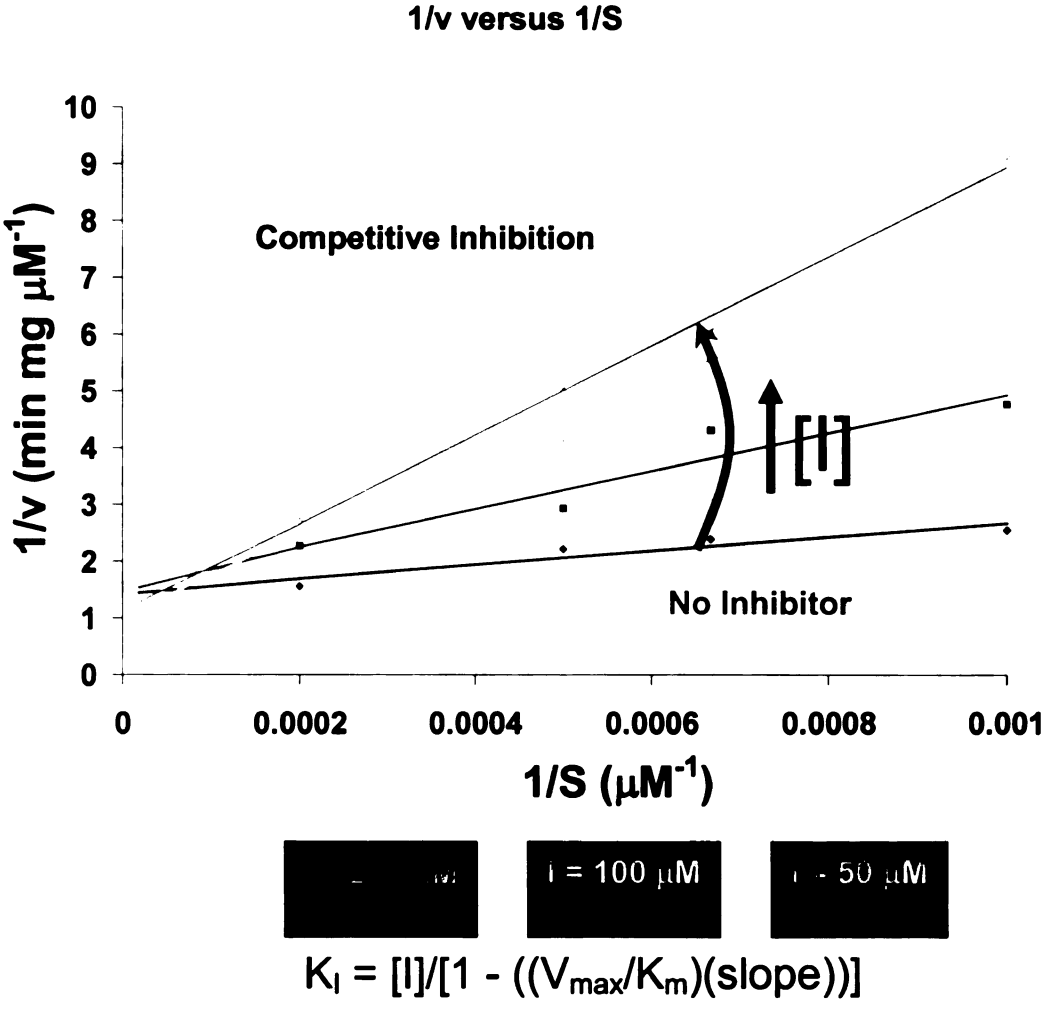

Figure 32. A double reciprocal plot to determine K_I and type of inhibition.

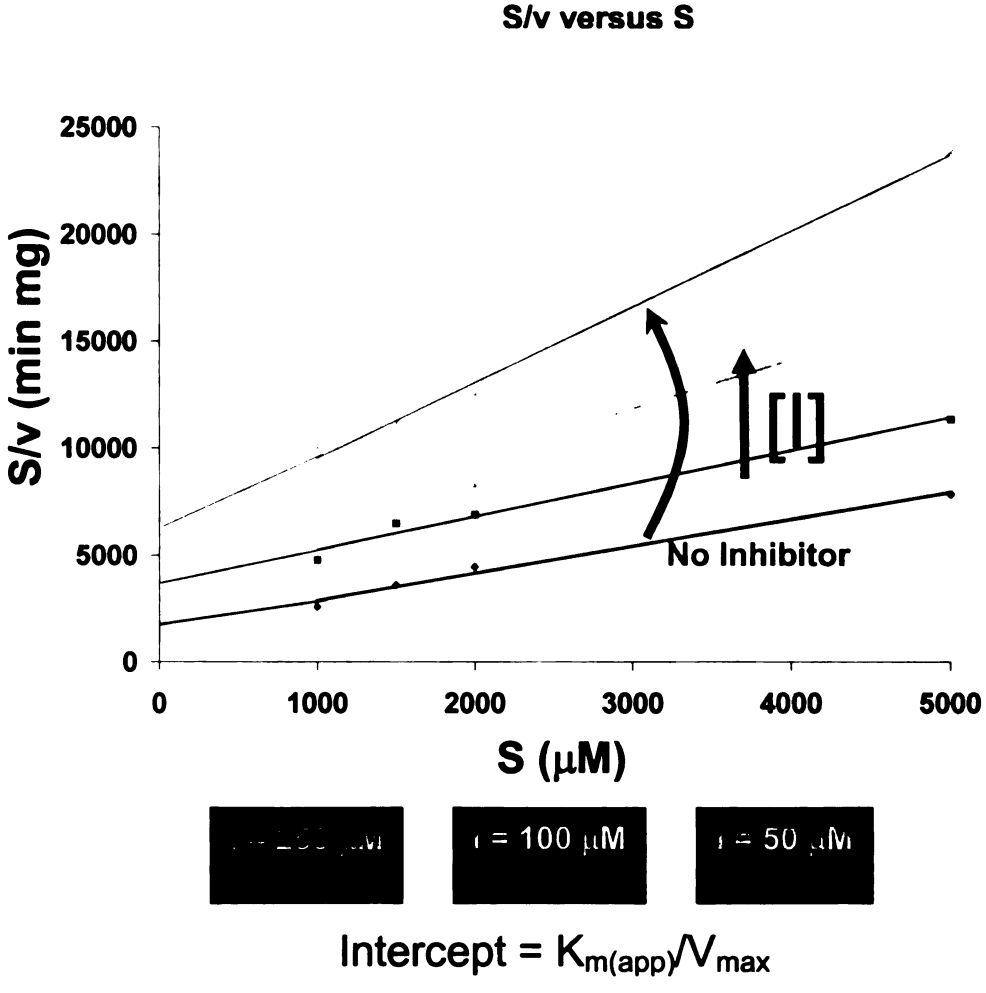

Figure 33. A plot of S/v versus S to determine the K_M/V_{max} value for the competitive inhibition equation used in calculating a K_I.

MATERIALS AND METHODS

Activity Assay Experimental to Determine the K_I for Valproate Inhibition

In order to determine the K_I for valproate inhibition, several plots are necessary. In this case, a simple OD_{595} versus time plot was used to determine the activity constant, an S/v versus S plot to determine the K_M/V_{max}, and a double reciprocal plot of 1/v versus 1/S to determine the type of inhibition and the final K_I. Similarly, as listed in Table 18, are all the components necessary for the assay experiment. The protocol used for the experiment went as follows:

(a) Incubate the enzyme assay solution, specific G6P concentration, and specific NAD^+ concentration at 37°C for ten minutes.
(b) Take out 100 μL of the assay solution and add 50 μL of 20% TCA to a new eppendorf tube. This is the time point at time 0.
(c) Add enzyme and inhibitor and reincubate for three minutes at 37°C. The typical amount of enzyme used was about 0.4-0.5 mg. The inhibitor concentrations ranged from 0 to 250 μM.
(d) After 3 minutes, take out another 100 μL sample and again, add to another new tube containing 50 μL of 20% TCA.
(e) Do this for 30 minutes taking 100 μL samples out every 3 minutes.
(f) After the 30-minute period, add 100 μL of 0.2 M $NaIO_4$ to each of the tubes containing a time point.
(g) Vortex the tubes and incubate them at 37°C for 30 minutes.
(h) After 30 minutes, add 150 μL of 1.5 M Na_2SO_3 and 600 μL of the P_i assay solution.
(i) Vortex the tubes again and incubate them at 42°C for 20 minutes.
(j) After 20 minutes, take the OD of each tube at 595 nm.
(k) Note: The tubes should gradually get a blue tint, which indicates the release of the phosphate from the product MIP. This is what is measured.

Table 18. Colorimetric assay components used in the determination of the K_I for valproic acid inhibition.

Enzyme Assay Solution
0.2 mM DTT
2 mM NH_4Cl
50 mM Tris HCl, pH=7.7

20% TCA
0.2 M $NaIO_4$
1.5 M Na_2SO_3

G6P
Various concentrations, ideal value, 5 mM

NAD^+
Various concentrations, ideal value, 1 mM

P_I assay solution
6:1 ratio of ammonium molybdate-Malachite green reagent to ascorbic acid

REFERENCES

1. Arganoff, B. W. and Fisher, S. K. (1991) *Inositol Phosphates and Derivatives*, Edited by A. B. Reitz, pp.20-32. Washington D.C.: American Chemical Society.

2. Majumder, A. L., Johnson, M. D., and Henry, S. A. (1997) *Biochim. Biophys. Acta*. **1348**(1-2), 245-256.

3. (a) Loewus, M. W., and Loewus, F. A. (1973) *Plant Sciences Letters*. **1**, 368-371. (b) Mauck, L. A., Wong, Y. H., and Sherman, W. R. (1980) *Biochemistry*. **19**(15), 3623-3629. (c) Pittner, F. and Hoffmann, O. O. (1978) *Hoppe Seyers Z. Physiol. Chem*. **359**(10), 1395-1400. (d) Sherman, W. R., Loewus, M. W., Pina, M. Z., and Wong, Y. H. (1981) *Biochim. Biophys. Acta*. **660**(2), 299-305.

4. (a) Abu-Abied, M. and Holland, D. (1994) *Plant Physiol*. **106**(4), 1689. (b) Dean-Johnson, A. and Henry, S. A. (1989) *J. Biol. Chem*. **264**(2), 1274-1283. (c) Ishitani, M., *et al.* (1996) *Plant J*. **9**, 279-293. (d) Johnson, M. D. (1994) *Plant Physiol*. **105**(3), 1203-1204. (e) Johnson, M. D. and Burk, D. H. (1995) *Plant Physiol*. **109**, 721. (f) Smart, C. C. and Fleming, A. J. (1996) *Plant J*. **4**, 279-293. (g) Wang, X. and Johnson, M. D. (1995) *Plant Physiol*. **110**, 336.

5. Altschul, S. F., *et al.* (1997) *Nucleic Acids Res*. **25**, 3389-3402.

6. (a) Loewus, M. W., Bedgar, D. L., and Loewus, F. A. (1984) *J. Biol. Chem*. **259**(12), 7644-7647. (b) Loewus, F. A., and Kelly, S. (1962) *Biochem. Biophys. Res. Commun*. **7**, 204-208.

7. (a) Belmaker, R. H., Berdsudsky, Y., Agam, G., Levine, J., and Koffman, O. (1996) *Annu. Rev. Med*. **47**, 47-56. (b) Berridge, M. J., Downes, C. P., and Hanley, M. R. (1982) *Biochem. J*. **206**, 587-595. (c) Berridge, M. J., and Irvine, R. F. (1989) *Nature*. **341**, 197-205.

8. (a) Koffman, O., *et al.* (1991) *Psychopharmacol. Bull*. **27**(3), 185-190. (b) Koffman, O., and Belmaker, R. H. (1990) *Brain Res*. **534**(1-2), 345-347.

9. Parthasarathy, R., and Eisenberg, G. J. (1991) *Inositol Phosphates and Derivatives*, Vol. 463, 1st Ed., Edited by A. B. Reitz, pp. 1-19. Washington D.C., American Chemical Society.

10. Exton, J. H. (1986) *Adv. Cyclic Nucleotide Protein Phosphorylation Res*. **20**, 211, 262.

11. Klig, L. S., and Henry, S. A. (1984) *Proc. Natl. Acad. Sci. U. S. A*. **81**(12), 3816-3820.

12. Griac, P., Swede, M. J., and Henry, S. A. (1996) *J. Biol. Chem.* **271**(41), 25692-25698.

13. Hirsch, J. P., and Henry, S. A. (1986) *Mol. Cell Biol.* **6**(10), 3320-3328.

14. Klig, L. S., Homann, M. J., Carman, G. M., and Henry, S. A. (1985) *J. Bacteriol.* **162**(3), 1135-11341.

15. Greeenberg, M. L., and Lopes, J. M. (1996) *Microbiol. Rev.* **60**, 1-20.

16. Nikoloff, D. M., and Henry, S. A. (1994) *J. Biol. Chem.* **269**(10), 7402-7411.

17. Hoshizaki, D. K., Hill, J. E., and Henry, S. A. (1990) *J. Biol. Chem.* **265**(8), 4736-4745.

18. White, M. J., Hirsch, J. P., and Henry, S. A. (1991) *J. Biol. Chem.* **266**(2), 863-872.

19. Klig, L. S., Hoshizaki, D. K., and Henry, S. A. (1988) *Curr. Genet.* **13**(1), 7-14.

20. Slekar, K. H., and Henry, S. A. (1995), *Nucleic Acids Res.* **23**(11), 1964-1969.

21. Lamping, E., Luckl, J., Paltauf, F., Henry, S. A., and Kohlwein, S.D. (1994) *Genetics.* **137**(1), 55-65.

22. Hudak, K. A., Lopes, J. M., and Henry, S. A. (1994) *Genetics.* **136**(2), 475-483.

23. Yoshida, K. T., Wada, T., Koyama, H., Mizobuchi-Fukuoka, R., and Naito, S. (1999) *Plant Physiology.* **119**, 65-72.

24. Johnson, M. D., and Wang, X. (1996) *J. Biol. Chem.* **271**(29), 17215-17218.

25. Nelson, D. E., Koukoumanos, M., and Bohnert, H.J. (1999) *Plant Physiology.* **119**, 165-172.

26. Nelson, D. E., Rammesmayer, G., and Bohnert, H. J. (1998) *Plant Cell.* **10**, 753-764.

27. Drobak, B. K., (1992) *Biochem. J.* **288**(Pt. 3), 697-712.

28. Lohia, A., Hait, N. C., and Majumder, A. L. (1999) *Mol. Biochem. Parasit.* **98**, 67-79.

29. Pittner, F., and Hoffmann-Ostenhof, O. (1979) *Mol. Cell Biochem.* **255**(18), 23-26.

30. Maeda, T., and Eisenberg, F. Jr. (1980) *J. Biol. Chem.* **255**(18), 8458-8464.

31. Mauck, L. A., Wong, Y. H., and Sherman, W. R. (1980) *Biochemistry.* **19**, 3623-3629.

32. Hasegawa, R., and Eisenberg, F., Jr. (1981) *Proc. Natl. Acad. Sci. U. S. A.* **78**, 4863-4866.

33. Bersudsky, Y., Kaplan, Z., Shapiro, Y., Agam, G., Kofman, O., and Belmaker, R. H. (1994) *Eur. Neuropsychopharmacol.* **4**(4), 463-467.

34. Benjamin, J., Agam, G, Levine, J., Bersudsky, Y., Kofman, O., and Belmaker, R. H. (1995) *Psychopharmacol. Bull.* **31**(1), 167-175.

35. Belmaker, R. H., Bersudsky, Y., Benjamin, J., Agam, G, Levine, J., and Kofman, O. (1995) *Adv. Biochem. Psychopharmacol.* **49**, 67-84.

36. Fux., M., Levine, J., Aviv, A., and Belmaker, R.H. (1996) *Am. J. Psychiatry.* **153**(9), 1219-1221.

37. Hussain, A., Bourgeois, J., Polvi, S., Tsang, E., Keller, W. A., and Georges, F. (1997) *Submitted.*

38. Fischer, D., and Eisenberg, D. (1996) *Protein Science.* **5**, 947-955.

39. Frey, P.A. (1987) in *Pyridine Nucleoside Coenzymes Part B.,* Vol. 2, Edited by D. Dolphin, R. Poulson, and O. Avramovic, pp. 461-511. New York, John Wiley & Sons.

40. Carpenter, E. P., Hawkins, A. R., Frost, J. W., and Brown, K. A. (1998) *Nature.* **394**, 299-302.

41. Thoden, J. B., Frey, P. A., and Holden, H. M. (1996) *Biochemistry.* **35**, 5137-5144.

42. Bauer, A. J., Rayment, I., Frey, P. A., and Holden, H. M. (1992) *Proteins: Struct. Func. Genet.* **12**, 372-381.

43. Thoden, J. B., Frey, P. A., and Holden, H. M. (1996) *Biochemistry.* **35**, 2557.

44. Migaud, M. E., and Frost, J. W. (1995) *J. Am. Chem. Soc.* **117**, 5154-5155.

45. Loewus, M. W., Loewus, F. A., Brillinger, G. U., Otsuka, H., and Floss, H. G. (1980) *J Biol. Chem.* **255**, 11710-11712.

46. Horecker, B. L., Tsolas, O., and Lai, C. Y. (1972) *The Enzymes*, Vol. 7, Edited by P.D. Boyer, pp. 213-258. New York, Academic Press.

47. Faber, K. (1997) *Biotransformations in Organic Chemistry*. Springer-Verlag, Berlin.

48. Littlechild, J. A., and Watson, J. C. (1993) *Trends in Biochemical Science*. **18**, 36-39.

49. Dreyer, M. K., and Schultz, G. E. (1996) *J. Mol. Biol.* **259**, 458-466.

50. Sherman, W. R., Loewus, M. W., Pina, M. Z., and Wong, Y. H. (1981) *Biochim. Biophys. Acta.* **660**(2), 299-305.

51. Creighton, T. E. (1993) *Proteins, Structure and Molecular Properties*. New York, W.H. Freeman and Co.

52. Wierenga, R. K., Terpstra, P., and Hol, W. G. (1986) *J. Mol. Biol.* **187**(1),101-107.

53. Vaden, D. L., Ding, D., Peterson, B., and Greenberg, M. L. (2001) *J. Biol. Chem.* **276**, 15466-15471.

54. Donahue, T. F., and Henry, S. A. (1981) *J. Biol. Chem.* **256**(13), 7077-7085.

55. Ames, B. N. (1966) *Methods Enzymol.* **8**, 115.

56. Migaud, M. E., and Frost, J. W. (1996) *J. Am. Chem. Soc.* **118**(3), 495-501.

57. Wlodawer, A., and Hodgson, K. O. (1975) *Proc. Natl. Acad. Sci. U. S. A.*, **72**, 398-399.

58. Otwinowski, Z., and Minor, W. (1997) *Methods Enzymol.* **276**, 307-326.

59. Matthews, B. W. (1968) *J. Mol. Biol.* **33**, 491-497.

60. Yang, W., Hendrickson, W. A., Kalman, E. T., and Crouch, R. J. (1990) *J. Biol. Chem.* **265**, 13553-13559.

61. Leahy, D. J., Erickson, H. P., Aukhil, I., Joshi, P., and Hendrickson, W. A. (1994) *PROTEINS, Structure, Function, and Genetics*. **19**,48-54.

62. Blundell, T. L. and Johnson, L. N. (1976) *Protein Crystallography*, Academic Press, New York.

63. Terwilliger, T. C., and Berendzen, J. (1999) *Acta Crystallogr.* D**55**, 849-861.

64. Collaborative Computational Project, No.4. (1994) *Acta Crystallogr.* D**50**, 760-763.

65. Drenth, J. (1994) *Principles of Protein X-ray Crystallography.* Springer, 292.

66. Jones, T. A., Zou, J. Y., and Kjelgard, M. (1991) *Acta Crystallogr.* A**47**, 110-119.

67. Brunger, A. T., Adams, P. D., Clore, G. M. DeLano, W. L., Gros, P., Grosse-Kunstleve, R. W., Jiang, J. S., Kuszewski, J., Nilges, M., Pannu, N. S., Read, R. J., Rice, L. M., Simonson, T., and Warren, G. L. (1998) *Acta Crystallogr.* D**54**, 905-921.

68. Laskowski, R. A., Macarthur, M. W., Moss, D. S., and Thornton, J. M. (1993) *J. Appl. Crystallogr.* **26**, 283-291.

69. Scapin, G., Cirilli, M., Reddy, S.G., Gao, Y., Vederas, J. C., and Blanchard, J. S. (1998) *Biochemistry.* **37**, 3278-3285.

70. Scapin, G., Reddy, S. G., and Blanchard, J. S. (1996) Biochemistry. 35, 13540-13551.

71. Stein, A. J., and Geiger, J. H. (2000) *Acta Crystallogr.* D**56**, 348-350.

72. Tian, F., Migaud, M. E., and Frost, J. W. (1999) J. Am. Chem. Soc.

73. Tian, F., Arthur, J. C., Peng, J., Migaud, M. E., and Frost, J. W. (1999) *Abstracts of Papers of the American Chemical Society.* **217**, U202.

74. Barnett, J. E. G., Rasheed, A., and Corina, D. L. (1973) *Biochem. Soc. Trans.* **1**, 1267.

75. Koshland, D. E., Jr. (1958) *Proc. Natl. Acad. Sci. U. S. A.* 44, 98-105.

76. Koshland, D. E. (1995) *Angew. Chem. Int. Ed. Eng.* **33**, 2375-2378.

77. Gerstein, M., Lesk, A. M., and Chothia, C. (1994) *Biochemistry* **33**, 6739 6749.

78. Benevides, J. M., Li, T. S., Lu, X. J., Srinivasan, A. R., Olson, W. K., Weiss, M. A., and Thomas, G. J. (2000) *Biochemistry* **39**, 548-556.

79. Pabo, C. O., and Sauer, R. T. (1992) *Annu. Rev. Biochem.* **61**, 1053-1095.

80. Weissman, M. M., Leaf, P. J., Tischler, G. L., Karno, M., Bruce, M. L., and Florio, L. P. (1988) *Psychol. Med.* **18**, 141-153.

81. Angst, J. (1986) *Psychopathology* **19**, Suppl. 2, 47-52.

82. American Psychiatry Association (1987) in *DSM-III-R: Diagnostic and Statistical Manual of Mental Disorders* (Williams, J. B. W., ed.) 3rd Ed., pp. 213-233, American Psychiatry Association, Washington, D. C.

83. Goodwin, F. K. and Jamison, K.R. (1990) *Manic-depressive Illness*, pp. 665-674, Oxford University Press, New York.

84. Chou, J. C. (1991) *J. Clin. Psychopharmacol.* **11**, 3-21.

85. Bowden, C. L., Brugger, A. M., Swann, A. A., Calabrese, J. R., Janicak, P. G., Petty, F., Dilsaver, S. C., Davis, J. J., Rush, A. J., and Small, J. G. (1994) *JAMA* **271**, 918-924.

86. Chen, G., Huang, L.-D., Jiang, Y.-M., and Manji, H. K. (1994) *J. Neurochem.* **63**, 2361-2364.

87. Manji, H. K., Bersudsky, Y., Chen, G., Belmaker, R. H., and Potter, W. Z. (1996) *Neuropsychopharmacology* **15**, 370-381.

88. Manji, H. K., Chen, G., Hsiae, J. K., Risby, E. D., Masana, M. I., and Potter, W. Z. (1996) *J. Clin. Psych.* **57**, 34-46.

89. Chen, G., Huang, L.-D., Jiang, Y.-M., and Manji, H. K. (1999) *J. Neurochem.* **72**, 1327-1330.

90. Chen, G. Yuan, P.-X., Jiang, Y.-M, Huang, L.-D., and Manji, H. K. (1999) *Mol. Brain Res.* **64**, 52-58.

91. Kendall, E. D., and Nahorski, S. R. (1997) *J. Pharmacol. Exp. Ther.* **241**, 1023-1027.

92. Casebolt, T. L., and Jope, R. S. (1989) *Bio. Psychiatry* **25**, 329-340.

93. Godfrey, P. P., McClue, S. J., White, A. M., Wood, A. J., and Grahame, S. D. (1989) *J. Neurochem.* **52**, 498-506.

94. Vadnal, R., and Parthasarathy, R. (1995) *Neuropsychopharmacology* **12**, 277-285.

95. Murray, M., and Greenberg, M. L. (2000) *Mol. Microbiol.* **36**, 651-661.

96. Li. R., Wing, L. L., Wyatt, R. J., and Kirsch, D. G. (1993) *Pharmacol. Biochem. Behav.* **46**, 323-329.

97. Dixon, J. F., and Hokin, L. E. (1997) *Proc. Natl. Acad. Sci. U. S. A.* **94**, 4757-4760.

98. Petsko, G. A. (1988) in *Diffraction Methods for Biological Macromolecules Part A*, Vol. 114, Edited by H. W. Wychoff, C. H. W. Hirs, and S. N. Tinnshef, pp. 147-156. Orlando, Academic Press.

99. Hendrickson, W. A., Horton, J. R., and LeMAster, D. M. (1990) *EMBO J.* **5**, 1665-1672.

100. Karle, J. (1980) *Int. J. Quant. Chem. Symp.* **7**, 357-367.

101. Barnett, J. E. G. and Corina, D. L. (1968) *Biochem. J.* **108**, 125.

102. Barnett, J. E. G., Rasheed, A., and Corina, D. L. (1973) *Biochem. J.* **131**, 21.

103. Loewus, M. W. (1977) *J. Biol. Chem.* **252**, 7221.

104. Sherman, W. R., Stewart, M. A., and Zinbo, M. (1969) *J. Biol. Chem.* **244**, 5703.

105. Kiely, D. E. and Sherman, W. R. (1975) *J. Am. Chem. Soc.* **97**, 6810.

106. Chen, C, H. –J. and Eisenberg, F. J. (1975) *J. Biol. Chem.* **250**, 2963.

107. Byun, S. N. and Jenness, R. (1981) *Biochemistry* **20**, 5174.

108. Manji, H. K., Moore, G. J., and Chen, G. (2001) *Brit. J. Psych.* **178** (suppl. 41), s107-s119.